



Published in final edited form as:

Dev Biol. 2022 June ; 486: 26–43. doi:10.1016/j.ydbio.2022.03.006.

Zebrafish mutants in *vegfab* can affect endothelial cell proliferation without altering ERK phosphorylation and are phenocopied by loss of PI3K signaling

Martin Lange^{1,2,4}, Nils Ohnesorge^{1,2}, Dennis Hoffmann^{1,2,6}, Susana F. Rocha⁵, Rui Benedito⁵, Arndt F. Siekmann^{1,2,3,*}

¹Max Planck Institute for Molecular Biomedicine, Roentgenstrasse 20, D-48149 Muenster, Germany

²Cells-in-Motion Cluster of Excellence (EXC 1003 – CiM), University of Muenster, Muenster, Germany

³Department of Cell and Developmental Biology and Cardiovascular Institute, Perelman School of Medicine at the University of Pennsylvania, Philadelphia, PA, USA

⁴current address: Cardiovascular Research Center, Yale University School of Medicine, CT, USA

⁵Centro Nacional de Investigaciones Cardiovasculares (CNIC), Madrid, E28029, Spain

⁶current address: Institute for Cell Biology, ZMBE, Von-Esmarch-Street 56, 48149 Muenster, Germany

SUMMARY

The formation of appropriately patterned blood vessel networks requires endothelial cell migration and proliferation. Signaling through the Vascular Endothelial Growth Factor A (VEGFA) pathway is instrumental in coordinating these processes. mRNA splicing generates short (diffusible) and long (extracellular matrix bound) Vegfa isoforms. The differences between these isoforms in controlling cellular functions are not understood. In zebrafish, *vegfaa* generates short and long isoforms, while *vegfab* only generates long isoforms. We found that mutations in *vegfaa* had an impact on endothelial cell (EC) migration and proliferation. Surprisingly, mutations in *vegfab* more strongly affected EC proliferation in distinct blood vessels, such as intersegmental blood vessels in the zebrafish trunk and central arteries in the head. Analysis of downstream signaling pathways revealed no change in MAPK (ERK) activation, while inhibiting PI3 kinase signaling phenocopied *vegfab* mutant phenotypes in affected blood vessels. Together, these results suggest

* Author for correspondence: Corresponding author: Dr. Arndt F. Siekmann, arndt.siekmann@pennmedicine.upenn.edu.

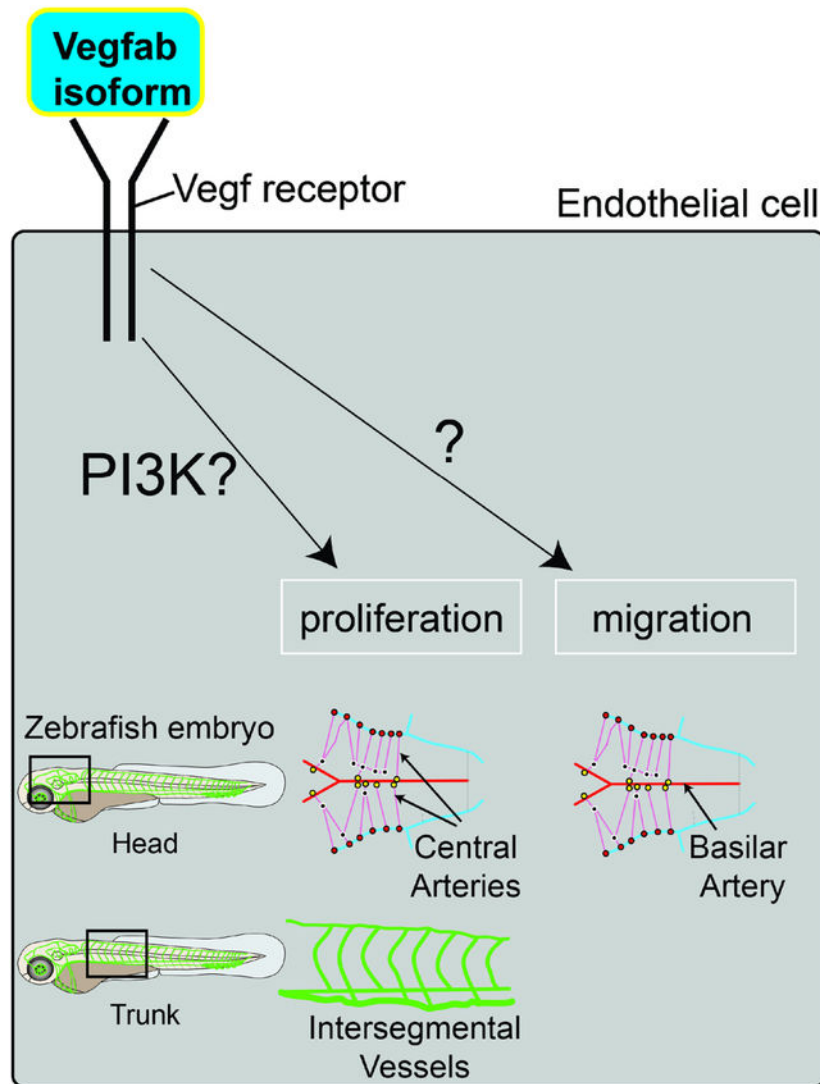
AUTHOR CONTRIBUTIONS

M.L. and A.F.S. conceived the experiments and analyzed the data. A.F.S. supervised the work. M.L. analyzed *vegfaa^{mu128}* and *vegfab^{mu155}* mutants, performed drug treatments and pERK stainings. A.F.S. cloned *vegfab¹⁷¹* and performed overexpression experiments. N.O. generated the *vegfaa^{mu128}* and *vegfab^{mu155}* mutants. D.H. analyzed data. S.F.R. performed mouse retina experiments and analyzed data. R.B. analyzed data of mouse retina. All authors discussed experiments and commented on the manuscript.

Publisher's Disclaimer: This is a PDF file of an unedited manuscript that has been accepted for publication. As a service to our customers we are providing this early version of the manuscript. The manuscript will undergo copyediting, typesetting, and review of the resulting proof before it is published in its final form. Please note that during the production process errors may be discovered which could affect the content, and all legal disclaimers that apply to the journal pertain.

that extracellular matrix bound Vegfa might act through PI3K signaling to control EC proliferation in a distinct set of blood vessels during angiogenesis.

Graphical Abstract



Keywords

zebrafish; angiogenesis; Vegf signaling; PI3 kinase signaling; endothelial cell proliferation

INTRODUCTION

The vascular system supplies our bodies with oxygen and nutrients to ensure efficient tissue homeostasis. In order to fulfil these functions, appropriate numbers of blood vessels need to be generated in the embryo or maintained during adulthood (Adams and Alitalo, 2007; Dejana et al., 2017; Potente et al., 2011). The overproduction of blood vessels can lead to

age-related macular degeneration (Mitchell et al., 2018), diabetic retinopathy (Wong et al., 2016) or cancer growth (Viallard and Larrivee, 2017). Formation of an insufficient number of blood vessels on the other hand can cause hypoxia, resulting in tissue damage as seen in atherosclerotic complication (Gimbrone and Garcia-Cardena, 2016).

Members of the vascular endothelial growth factor (VEGF) family are established regulators of vascular development (Alvarez-Aznar et al., 2017; Koch and Claesson-Welsh, 2012; Simons et al., 2016). For instance, the formation of new blood vessels from pre-existing ones, termed angiogenesis, heavily relies on VEGFA and its receptor VEGFR2 (Kdr or Flk1). Accordingly, heterozygous *Vegfa* mutant mice die in utero with vascular defects (Carmeliet et al., 1996; Ferrara et al., 1996). Subsequent studies showed that VEGFA controls differentiation, sprouting, migration, proliferation and survival of ECs. Despite the identification of several downstream players, such as Phosphoinositide 3-kinase (PI3K) (Graupera and Potente, 2013) and Mitogen-activated protein kinase (MAPK/ERK) (Simons *et al.*, 2016), it is not known how VEGF signaling can differentially activate these pathways and how this activation might lead to the observed broad array of cellular outcomes. For example, the PI3K pathway controls EC survival in response to VEGFA in cultured cells (Gerber et al., 1998; Nakatsu et al., 2003), while *in vivo* studies in the developing mouse retina (Graupera et al., 2008) and in zebrafish embryos (Nicoli et al., 2012) suggested that PI3K signaling predominantly regulates EC migration. More recent studies, however, also suggested a function of PI3K signaling in EC proliferation during retinal development (Angulo-Urarte et al., 2018; Ola et al., 2016) and in vascular malformations (Castel et al., 2016; Castillo et al., 2019; Castillo et al., 2016). Further work in mouse and in cell culture has shown that ERK signaling downstream of VEGFA stimulates EC proliferation (Koch and Claesson-Welsh, 2012), vessel integrity (Ricard et al., 2019) and artery formation (Simons and Eichmann, 2015). Another study in zebrafish embryos, however, implicated ERK signaling mainly in regulating EC migration, being dispensable for early artery differentiation (Shin et al., 2016). Therefore, we still lack an understanding of the sequence of downstream VEGF signaling events that occur during blood vessel formation. We also do not understand how these might be triggered in different EC populations through differential ERK and PI3K signaling.

One key aspect of VEGFA biology is the existence of differentially spliced isoforms (Bowler and Oltean, 2019). Longer isoforms bind heparin and are associated with the extracellular matrix (ECM), while the short, 121 amino acid (aa) isoform is diffusible (Vempati et al., 2014). Studies in mice have shown that these isoforms differentially affect blood vessel formation. Genetically engineered mice, which only express the VEGFA165 isoform are viable (Stalmans et al., 2002), while mice expressing only VEGFA121 show angiogenesis defects (Carmeliet et al., 1999; Ruhrberg et al., 2002; Stalmans *et al.*, 2002). Thus, the ability to associate with the extracellular matrix might change VEGFA downstream signaling and/or gradient formation, as shown in cultured cells (Chen et al., 2010).

Zebrafish contain two *vegfa* paralogs, *vegfaa* and *vegfab*, likely being generated during a genome duplication event (Taylor et al., 2003; Taylor et al., 2001). Both genes are expressed during early embryogenesis and encode differentially spliced gene products, with *vegfaa* encoding 121- and 165 aa isoforms (Gong et al., 2004; Liang et al., 1998), and *vegfab*

encoding 171 and 210 aa isoforms (Bahary et al., 2007). Therefore, while *vegfaa* generates both diffusible and ECM bound isoforms, *vegfab* only generates ECM bound isoforms. Here, we have generated zebrafish mutants for *vegfaa* and *vegfab*. We find that, in agreement with studies in mice, *vegfaa* is haploinsufficient. By contrast, *vegfab* mutants showed only mild vascular defects and survived to adulthood. However, EC proliferation was similarly affected in *vegfab* mutants. Using inhibitor treatments and time-lapse analysis of vascular development, we show that inhibiting PI3K signaling phenocopied the proliferation defects observed in *vegfab* mutants without major alterations in ERK activation. We also show that inhibition of PI3K signaling in the mouse retina similarly affected EC proliferation. Together, our studies support a model, in which activation of PI3K signaling downstream of ECM bound VEGFA might allow for optimal EC proliferation during angiogenesis of distinct sets of blood vessels that is independent of signaling through ERK.

RESULTS

***Vegfaa* and *vegfab* mutants show distinct defects during brain blood vessel formation**

In order to investigate the role of each of the zebrafish *Vegfa* homologues during angiogenesis, we generated zinc finger (for *vegfaa*) or TALEN (for *vegfab*) mutants, targeting the first exon of either gene. We recovered two frameshift mutations, leading to severely truncated proteins of 18 (*vegfaa^{mu128}*) or 12 amino acids (*vegfab^{mu155}*), respectively (Figure 1A, B). To assess changes in vascular morphology, we crossed both mutant lines into the *Tg(kdrl:EGFP)^{s843}* background, expressing EGFP in ECs (Jin et al., 2005). We first focused our analysis on the developing hindbrain vasculature (Figure 1C), which relies on VEGFR2 signaling (Bussmann et al., 2011; Fujita et al., 2011; Ulrich et al., 2011). The arterial pole of the hindbrain vasculature forms via two successive sprouting events emanating from the primordial hindbrain channels (PHBC), two laterally located veins (Bussmann et al., 2011; Fujita et al., 2011; Ulrich et al., 2011). The first sprouting event generates the medially located basilar artery (BA), while the second event subsequently generates central arteries (CtAs), which connect the PHBCs with the BA (Figure 1D–F; Video S1). Both *vegfa* genes show distinct expression domains in the brain, as shown by fluorescence in situ hybridization at 32 hpf. We detected expression of *vegfaa* dorsal to the PHBC at positions of forming CtAs (Supplementary Figure S1A, arrows, B). For *vegfab*, expression was evident in the midline region, where the BA would form (Supplementary Figure S1C, arrowheads, D) and dorsally of the PHBCs (Supplementary Figure S1C, arrows, D).

In line with these gene expression data, we observed specific vascular defects in each mutant. Homozygous *vegfaa^{mu128}* mutants showed a significant decrease in CtA numbers, while these were unaffected in *vegfab^{mu155}* mutants (Figure 1G–L, quantified in Figure 1P; Videos S2 and S3). By contrast, the BA failed to form in these mutants, as previously reported (Rossi et al., 2016). Its formation was unaffected in *vegfaa^{mu128}* mutants (Figure 1G–L). To analyze whether *vegfab* can contribute to CtA formation, we analyzed *vegfaa^{mu128}; vegfab^{mu155}* double mutants. These showed a complete lack of BA and CtAs, while the PHBCs still formed (Figure 1M–O, quantified in Figure 1P). These results suggest that during brain blood vessel sprouting, *vegfaa* and *vegfab* have acquired specific regulatory

elements that drive their expression in separate domains, thereby locally influencing blood vessel formation.

Mutant hindbrain phenotypes display cell number changes in particular blood vessels

Angiogenesis requires the coordination of EC migration and proliferation (Adams and Alitalo, 2007; Hogan and Schulte-Merker, 2017; Potente *et al.*, 2011; Schuermann *et al.*, 2014). We therefore set out to investigate the influence of either *vegfa* gene on these processes. To do so, we quantified cell numbers using the double transgenic line *Tg(kdrl:Hsa.HRAS-mCherry)⁹¹⁶; Tg(fli:nEGFP)⁷*, in which EC nuclei contain EGFP protein and membranes are labelled by virtue of mCherry expression (Hogan *et al.*, 2009; Roman *et al.*, 2002). After completion of BA and CtA sprouting (58 hpf time point), both mutants displayed lower total cell numbers when compared to wildtype (wt) embryos (Figure 1Q–T). Further analysis revealed that neither *vegfaa^{mu128}* nor *vegfab^{mu155}* affected PHBC cell numbers (Figure 1U). As expected, BA cell numbers were specifically affected in *vegfab^{mu155}* mutants (Figure 1V). This contrasted with *vegfaa^{mu128}* mutants, which did not show differences in BA cell numbers (Figure 1V). The amounts of CtAs decreased about 50% in *vegfaa^{mu128}* mutants (Figure 1R, quantified in Figure 1P) and accordingly, total CtA cell numbers were also reduced in these mutants (Figure 1W). Surprisingly however, total CtA cell numbers were similarly decreased in *vegfab^{mu155}* mutants when compared to wt embryos (Figure 1W), even though *vegfab^{mu155}* mutants formed normal numbers of CtAs (Figure 1P). We therefore reasoned that *vegfab* might affect EC numbers in individual CtAs. Indeed, while individual CtAs in *vegfaa^{mu128}* mutants contained similar quantities of ECs compared to wt embryos, cell numbers per CtA in *vegfab^{mu155}* were significantly decreased (Figure 1X). Together, these findings suggest that, depending on their expression pattern, *vegfaa* and *vegfab* can both control EC migration. In addition, *vegfab* can affect EC proliferation in distinct sets of blood vessels without major influences on EC migration.

Vegfab signaling is required for EC proliferation

To test this hypothesis, we leveraged the accessibility of zebrafish for time lapse imaging. We used *Tg(kdrl:Hsa.HRAS-mCherry)⁹¹⁶; Tg(fli:nEGFP)⁷* embryos to track the proliferative behaviors of individual ECs. In wt embryos, we observed CtA EC proliferation between 32 and 42 hpf (Supplementary Figure S1E, white dots; Video S4). Ultimately, 16.5 % of CtA cells were derived from a cell division (Supplementary Figure S1H, I). Although fewer CtAs sprouted in *vegfaa^{mu128}* mutants, the ones that formed displayed a similar percentage of CtA cells derived from proliferation when compared to wt embryos (Supplementary Figure S1F, white dots, quantified in Supplementary Figure S1H, I; Video S5). By contrast, *vegfab^{mu155}* mutants showed a reduction of cells derived from proliferation to 3.4 % (Supplementary Figure S1G, white dots, quantified in Figure S1H, I; Video S6). Thus, *vegfaa* signaling cannot compensate for loss of *vegfab* signaling in stimulating EC proliferation during CtA sprouting.

We further tested the ability of *vegfab* in regulating EC proliferation through ubiquitous overexpression using mRNA injections. Injecting 50 pg of *vegfab₁₇₁* mRNA into one cell zebrafish embryos did not lead to major vascular patterning defects, but increased EC numbers in CtAs (Figure 2A–F, quantified in Figure 2G) and BA (Figure 2H–M, quantified

in Figure 2N). Together, these findings suggest that *vegfab* signaling might be critically required in controlling EC proliferation.

ECs from alternate sources can rescue BA formation in *vegfab^{mu155}* mutant embryos

Despite defects in BA morphogenesis and a reduction in brain EC numbers, *vegfab^{mu155}* mutants can survive to adulthood. This suggests that compensatory mechanisms might repair early developmental defects. Indeed, we observed that at 72 hpf a BA had formed in *vegfab^{mu155}* mutant embryos, about one day later than in wt embryos (Figure 3). The BA in *vegfab^{mu155}* mutants displayed normal length (Figure 3A, B, quantified in Figure 3C), diameter (Figure 3D, E, quantified in Figure 3F) and cross-sectional area (Figure 3G) when compared to wt embryos. However, BA cell numbers (Figure 3H) and BA cells/area (Figure 3I) were still markedly reduced in mutant embryos.

We then set out to determine the source of ECs that might contribute to BA formation in *vegfab^{mu155}* mutants. We reasoned that later forming CtA sprouts that connect to the BA in wt embryos might contribute cells to the BA in *vegfab^{mu155}* mutants. We previously showed that proper CtA sprouting relied on *cxcr4a* signaling without affecting BA formation (Bussmann *et al.*, 2011) (Figure 3J, K, N). To test whether CtA cells could contribute to BA formation, we knocked down *cxcr4a* expression through morpholino injection. This led to a failure of BA rescue in *vegfab^{mu155}* mutants, suggesting that CtA cells can compensate for a lack of EC sprouting from the PHBCs during early BA formation in *vegfab^{mu155}* mutants (Figure 3J–N). However, the rescue was not complete, as EC numbers were lower in rescued BAs (Figure 3N). Together, these findings illustrate the plasticity of the brain vasculature and the ability of brain ECs to contribute to alternate vessels, as was also shown for the great vessels of the heart (Nagelberg *et al.*, 2015).

VEGFab and VEGFaa differentially affect intersegmental blood vessel sprouting

To corroborate our findings, we analyzed the morphology of intersegmental blood vessels (ISVs), the first blood vessels that form via angiogenesis in the trunk of zebrafish embryos (Isogai *et al.*, 2003). Analysis of *vegfaa₁₂₁* and *vegfab₁₇₁* expression at 28 and 32 hpf revealed expression of *vegfaa₁₂₁* in somitic tissue, being strongest in regions of newly emerging blood vessel sprouts at 28 hpf (Supplementary Figure S2A, B). Additional expression domains at 28 and 32 hpf included dorsal regions in the vicinity of the DLAV (Supplementary Figure S2A–D, arrows) and the pronephros (Supplementary Figure S2C asterisks). By contrast, expression of *vegfab₁₇₁* was mainly detected in dorsal regions (Supplementary Figure S2E–H, arrows). In wt embryos, ISVs sprout from the dorsal aorta and anastomose in the dorsal region of the zebrafish trunk at 30 hpf, forming the dorsal longitudinal anastomotic vessel (DLAV) (Isogai *et al.*, 2003) (Supplementary Figure S3A, B, quantified in Supplementary Figure S3K). *vegfaa^{mu128}* heterozygous embryos showed a variable degree of stalled ISVs (Supplementary Figure S3C, D, arrowhead, quantified in Supplementary Figure S3K), indicating haploinsufficiency, as previously reported for VEGFA mutant mice (Carmeliet *et al.*, 1996). ISVs failed to form in *vegfaa^{mu128}* homozygous embryos (Supplementary Figure S3E, F, quantified in Supplementary Figure S3K), as shown earlier for independently generated *vegfaa^{bns1}* mutants (Rossi *et al.*, 2016). Surprisingly, neither *vegfab^{mu155}* heterozygous nor homozygous mutants showed defects

in ISV morphology at 30 hpf (Supplementary Figure S3G–J, quantified in Supplementary Figure S3K). These results thus underscore a conserved role of *vegfaa* signaling during ISV formation, while *vegfab* appears to be dispensable during this process.

Motivated by our observations concerning the distinct phenotypes of *vegfaa* and *vegfab* in forming CtAs, we set out to determine whether *vegfab* might similarly affect EC proliferation in ISV ECs. As previously reported, wt embryos contained either 3 or 4 cells per ISV (Figure 4A, B, quantified in Figure 4G), (Childs et al., 2002; Costa et al., 2016; Siekmann and Lawson, 2007). ISVs in *vegfaa^{mu128/+}* mutants contained significantly fewer ECs (Figure 4C, D, quantified in Figure 4G). *Vegfab^{mu155}* mutants displayed a reduction in ISV EC numbers (Figure 4E, F, quantified in Figure 4G) with only minor sprouting defects. Thus, similar to brain CtAs, loss of *vegfab* leads to a reduction in ISV cell numbers. We then interrogated the effect of *vegfab₁₇₁* overexpression on ISV cell numbers. Injecting 50 pg of *vegfab₁₇₁* mRNA did not cause major defects in ISV morphology, but increased EC numbers (Supplementary Figure S4A, B, quantified in Supplementary Figure S4E). In addition, *vegfab₁₇₁* mRNA injection could rescue EC number defects in *vegfab^{mu155}* mutant embryos (Supplementary Figure S4C, D, quantified in Figure S4E). Thus, comparable to our observations for the hindbrain vasculature, overexpression of *vegfab₁₇₁* can lead to an increase in EC numbers also in trunk blood vessels.

In order to investigate whether ISV phenotypes would resolve in *vegfab^{mu155}* mutants, we followed ISV development over time. At the 48 hpf time point, we continued to observe a reduction in EC numbers, both in arterial and venous ISVs (Supplementary Figure S5A–F, quantified in Supplementary Figure S5G, H). There was no difference between wt embryos and *vegfab^{mu155}* mutants in respect to the number of arterial ISVs (Supplementary Figure S5I), while the number of uperfused ISVs was increased (Supplementary Figure S5J). At the 72 hpf time point, only venous ISVs showed a reduction in EC numbers (Supplementary Figure S5K–P, quantified in Supplementary Figure S5Q, R). There was no change in artery-vein ISV patterning (Supplementary Figure S5S), while the number of unperfused ISVs remained about twice as high in *vegfab* mutants when compared to wt embryos (Supplementary Figure S5T). Together, these results suggest that *vegfab* signaling is required in distinct sets of blood vessels to allow for optimal EC proliferation and proper perfusion of the vascular network.

To analyze the phenotypic differences between *vegfaa^{mu128}* and *vegfab^{mu155}* mutants with respect to EC migration and proliferation, we performed time-lapse imaging of *Tg(kdrl:Hsa.HRAS-mCherry)^{s916}*, *Tg(fli:nEGFP)^{y7}* zebrafish embryos. As determined by nuclear displacement, wt tip cells on average migrated about 100 μ m within 6 h (Figure 4H, arrowheads, quantified in Figure 4L; Video S7), as previously reported (Costa et al., 2016). By contrast, ISVs in *vegfaa^{mu128/+}* fish displayed two different behaviors: Tip cells either migrated like wt cells (Figure 4I, quantified in Figure 4L; Video S8), or showed severe migration defects with tip cells stalling midway along the somite (Figure 4J, quantified in Figure 4L; Video S9). Therefore, lack of one *vegfaa* allele can differentially affect individual ISVs. *Vegfab^{mu155}* mutants showed a decrease in cell migration in the midway position, but later recovered and reached the dorsal region of the embryo at the same time as the wt cells did (Figure 4K, quantified in Figure 4L; Video S10). Therefore, absence of *vegfaa* signaling

can have strong effects on EC migration, while the effects of *vegfab* on cell migration are less pronounced.

By contrast, EC proliferation was affected in both *vegfaa*^{mu128/+} and *vegfab*^{mu155} mutants. Time-lapse imaging revealed that in wt embryos each ISV showed around one EC proliferation event (Figure 4M, quantified in Figure 4P; Video S11). This was reduced to about half for both *vegfaa*^{mu128/+} mutants (Figure 4N, quantified in Figure 4P; Video S12) and *vegfab*^{mu155} (Figure 4O, quantified in Figure 4P; Video S13) mutants. In summary, our findings suggest that *vegfaa* signaling drives EC migration and proliferation, while *vegfab* signaling more strongly affects EC proliferation, both in ISVs and CtAs.

To further investigate the different cellular functions of *vegfaa* and *vegfab*, we asked whether overexpressing the short *vegfaa*₁₂₁ isoform would similarly lead to an increase in EC numbers. Injection of 50 pg of *vegfaa*₁₂₁ disrupted trunk vascular patterning and ISV morphogenesis (Supplementary Figure S6A–F), as previously reported for co-injections of *vegfaa*₁₂₁ and *vegfaa*₁₆₅ mRNA (Casie Chetty et al., 2017). This phenotype precluded an analysis of ISV EC numbers. We then aimed at titrating down *vegfaa*₁₂₁ mRNA amounts to levels that would allow for normal ISV sprouting. A dose of 10 pg *vegfaa*₁₂₁ did not affect ISV development but also did not lead to an increase in EC numbers within ISVs (Supplementary Figure S6G–L, quantified in Supplementary Figure 6M). Thus, because of the influence of *vegfaa*₁₂₁ overexpression on ISV morphogenesis, we cannot determine whether this isoform affects EC proliferation in a similar manner as *vegfab*₁₇₁ does.

Overexpression of *vegfab*₁₇₁ can rescue *vegfaa*^{mu128} mutant phenotypes

To further analyze similarities between *vegfaa* and *vegfab* signaling, we subsequently asked whether *vegfab*₁₇₁ overexpression could rescue *vegfaa*^{mu128} mutant embryos. Previous studies showed that *vegfab*₁₇₁ was unable to rescue *vegfaa*^{bns1} mutant embryos, except when the *vegfab*₁₇₁ signal peptide was being replaced by that of *vegfaa*₁₆₅ (Rossi et al., 2016). Surprisingly, the *vegfab*₁₇₁ clone we used for generating mRNA was able to rescue various aspects of the *vegfaa*^{mu128} mutant phenotype. This independently generated clone contained the endogenous 5' UTR of *vegfab*₁₇₁ (see Materials and Methods). We observed an almost complete rescue of lateral dorsal aorta formation and discernable dorsal aortae and posterior cardinal veins (Supplementary Figure S7A–H, quantified in Supplementary Figure S7I). We also observed trunk circulation at 48 hpf in about a quarter of injected *vegfaa*^{mu128} mutant embryos (Supplementary Figure S7I). Sprouting of ISVs was rescued to a lesser extent (Supplementary Figure S7H, quantified in Supplementary Figure S7J) and the rescue was limited to the most anterior regions of the embryo. Thus, while *vegfab*₁₇₁ could compensate for arterial morphogenesis defects in *vegfaa*^{mu128} mutants, rescue of ISV sprouting was more moderate.

Vegfab controls EC proliferation independently of ERK signaling

We reasoned that the observed differences in EC behaviors between *vegfaa*^{mu128} and *vegfab*^{mu155} mutants might enable us to dissect out signaling pathways downstream of Vegfa that specifically control proliferation. Previous studies implicated signaling through MAPK/ERK in influencing EC proliferation (Claesson-Welsh, 2016; Simons et al., 2016).

We therefore set out to determine potential changes in ERK phosphorylation in *vegfab^{mu155}* mutants. Surprisingly, pERK antibody staining in ISVs did not show major differences in *vegfab^{mu155}* mutant embryos (Figure 5A, B, quantified in Figure 5C and Supplementary Figure S8A–G). ERK signaling furthermore influences gene expression patterns within ISVs (Shin *et al.*, 2016). We did not detect changes in either of the two reported ERK downstream genes *dll4* (Figure 5D–G) or *flt4* (Figure 5H–K) in *vegfab^{mu155}* mutants. Lastly, treating wt embryos with phorbol 12-myristate 13-acetate (PMA), which increased ERK phosphorylation (Supplementary Figure S9A–C), did not change EC numbers within ISVs (Figure 5L–Q, quantified in Figure 5X). PMA treatment also failed to rescue EC numbers in *vegfab^{mu155}* mutants (Figure 5R–W, quantified in Figure 5X). Therefore, our results suggest that ERK signaling does not play a major role downstream of *vegfab* signaling in controlling EC proliferation in ISVs.

Previous studies in zebrafish suggested that signaling through ERK is required for ISV sprouting (Shin *et al.*, 2016). The authors furthermore showed a reduction in pERK staining in embryos mutant for Vegfa pathway components, such as *kdrl* and *plcg* or treated with a Vegf receptor inhibitor (Shin *et al.*, 2016). We therefore reasoned that activation of ERK phosphorylation might rescue EC migration and ISV sprouting in *vegfaa^{mu128}* mutant embryos. However, PMA treatment of *vegfaa^{mu128}* mutants failed to rescue ISV sprouting (Supplementary Figure S10A–F). Thus, acute activation of ERK signaling is not sufficient to induce EC sprouting in *vegfaa^{mu128}* mutants.

Loss of PI3K signaling specifically affects EC proliferation

We next focused on PI3K signaling, as another important pathway downstream of VEGFA signaling (Graupera and Potente, 2013). Since we could not directly visualize potential alterations in PI3K signaling activity within ECs during ISV sprouting due to the lack of a robust immunohistochemistry protocol, we chose to inhibit PI3K signaling pharmacologically and analyze the resulting vascular phenotypes. Treating zebrafish embryos with 10 μ M of the PI3K inhibitor LY294002 (Vlahos *et al.*, 1994) reduced phosphorylation of the PI3K downstream kinase AKT without affecting gross embryonic morphology (Supplementary Figure S11A–C). ISV morphology was unaffected when treating zebrafish embryos from 22 to 32 hpf (Figure 6A, D). However, similar to *vegfab^{mu155}* mutants, EC numbers were significantly reduced in inhibitor treated embryos when compared to DMSO treated control embryos (Figure 6B, C, E, F, quantified in Figure 6G). We then investigated whether this reduction in cell numbers was due to the reported effects of PI3K signaling on cell migration. Surprisingly, time-lapse imaging of developing ISVs did not reveal changes in cell migration upon LY294002 treatment (Figure 6H, I, quantified in Figure 6J; Videos S14 and S15). We therefore investigated EC proliferation in inhibitor treated embryos. This analysis revealed that blocking PI3K signaling led to a decrease in proliferation events (Figure 6K, L, quantified in Figure 6M; Videos S16 and S17). As LY294002 inhibits multiple PI3K isoforms in addition to other kinases (Davies *et al.*, 2000; Workman *et al.*, 2010), we investigated ISV formation after treating embryos with the PI3K p110 α isoform specific inhibitor GDC-0326 (Heffron *et al.*, 2016). GDC-0326 treatment effectively reduced AKT phosphorylation at concentrations ranging from 10 μ M to 50 μ M (Supplementary Figure S12A) and reduced ISV cell numbers without affecting ISV

morphology (Supplementary Figure S12B–M, quantified in Supplementary Figure S12N), as also recently shown (Angulo-Urarte *et al.*, 2018). Thus, while not affecting ISV EC migration during short term inhibitor treatment, PI3K signaling downstream of the 110 alpha isoform plays important roles in controlling EC proliferation during developmental angiogenesis.

Since our results suggested distinct functions of *vegfaa* and *vegfab* during brain blood vessel development, we interrogated the effect of inhibiting PI3K signaling on BA and CtA formation. Interestingly, treating wt embryos from 24 hpf to 48 hpf with GDC-0326 did not affect BA sprouting or BA cell numbers (Supplementary Figure S13A–F, quantified in Supplementary Figure S13G). BA formation was also unaltered in GDC-0326 treated *vegfaa^{mu128}* mutants (Supplementary Figure S13H–N). These findings suggest that *vegfab* is the sole Vegfa ligand responsible for BA formation and in this setting does not work through PI3 kinase activation. We then analyzed the effect of PI3K inhibition on CtA formation, which rely on both Vegfaa and Vegfab signaling. Here, we observed a reduction in CtA EC numbers in PI3K inhibitor treated embryos (Supplementary Figure S14A–F, quantified in Supplementary Figure S14G). This reduction was comparable to what we had observed in *vegfab^{mu155}* mutants (Figure 1X). Inhibition of PI3K signaling did not further reduce CtA numbers in *vegfaa^{mu128}* mutants (Supplementary Figure S14H–M, quantified in Supplementary Figure S14 N). Thus, in CtAs, inhibition of PI3K signaling phenocopied loss of *vegfab*, similar to what we had observed during ISV sprouting.

The finding that PI3K inhibition did not further reduce CtA EC numbers in *vegfaa^{mu128}* embryos was surprising, as it suggests that in the absence of Vegfaa signaling, Vegfab does not function through activating PI3K. To further investigate this possibility, we asked whether reducing PI3K signaling would exacerbate ISV phenotypes in *vegfaa^{mu128}* mutant embryos. Since homozygous mutants completely lack ISVs, precluding the analysis of a possible interaction, we treated heterozygous *vegfaa^{mu128}* animals with GDC-0326 and analyzed ISV phenotypes at 48 hpf (Figure 7A–E). These experiments showed that inhibition of PI3K in *vegfaa^{mu128}* heterozygous animals led to a greater reduction in EC numbers when compared to either heterozygous or inhibitor treated animals alone (quantified in Fig. 7E). Thus, in ISVs additional loss of PI3K signaling increases *vegfaa^{mu128}* mutant phenotypes. Since we cannot rule out that the remaining wildtype *vegfaa* allele might signal through PI3K, we devised an experimental strategy to directly test the effect of PI3K inhibition on Vegfab signaling. To do so, we injected *vegfab₁₇₁* mRNA and subsequently treated animals with GDC-0326 (Fig. 7F–L). Injection of *vegfab₁₇₁* mRNA increased ISV cell numbers (Fig. 7L), as noted before (Supplementary Fig. S4). Inhibiting PI3K function in these embryos reduced this response (Figure 7L). However, ISV cell numbers in *vegfab₁₇₁* injected and GDC-0326 treated embryos were still higher than in either uninjected or control mRNA injected embryos treated with GDC-0326 (Figure 7L). Therefore, blocking PI3K signaling only partially abrogated the effect on EC proliferation normally observed when increasing Vegfab₁₇₁ ligand availability. Because of this result we cannot firmly conclude that Vegfab acts solely through PI3K signaling in ISVs to increase EC proliferation.

Inhibition of PI3 kinase signaling during retinal angiogenesis reduces EC proliferation

To investigate whether PI3K signaling influences EC proliferation in other angiogenic settings, we analyzed blood vessel development in the mouse retina. Here, new blood vessels sprout from the optic nerve towards the periphery of the retina after birth. Intraperitoneal injection of the PI3K 110 alpha subunit-specific inhibitor GDC-0941 effectively reduced AKT phosphorylation after 24 h of treatment, as analyzed in lung lysates from P6 mice (Supplementary Figure S15A). It furthermore reduced the phosphorylation of S6 kinase, a downstream target of PI3K signaling (Chung et al., 1994) (Supplementary Figure S15B–E). Incorporation of EdU was strongly reduced in inhibitor treated embryos, both at the angiogenic front (Figure 8A–D, quantified in Figure 8G) and in the vein region of the retina (Figure 8E, F, quantified in Figure 8H), where ECs continue to proliferate. Thus, similar to our observations in zebrafish embryos, PI3K signaling affects EC proliferation during mouse retinal angiogenesis.

DISCUSSION

Tissue vascularization requires coordinated cellular responses to growth factors, such as Vegfa, in order to generate appropriate amounts of new ECs, allow them to sprout into avascular areas and ultimately differentiate into the correct numbers of arteries, capillaries and veins. How a single ligand can control the multitude of cellular responses necessary to achieve these tasks is an outstanding question in the field. Our work on the duplicated Vegfa ligands in zebrafish suggests a function of PI3 kinase signaling in response to ECM bound *vegfab* ligands in regulating EC proliferation. This was an unexpected discovery, since signaling through MAPK/ERK was thought to be the main driver of EC proliferation downstream of Vegfa signaling (Koch and Claesson-Welsh, 2012; Meadows et al., 2001; Simons *et al.*, 2016; Srinivasan et al., 2009; Takahashi et al., 1999). What might be the reason for this discrepancy? So far, animal models carrying mutations in components of the Vegf pathway showed simultaneous defects in EC proliferation and migration. For instance, zebrafish mutants in *kdr1*, *plcg* or treated with the Vegf pathway inhibitor SU5416 display an absence of ERK phosphorylation (Fish et al., 2017; Shin *et al.*, 2016), together with a reduction in ISV outgrowth and cell numbers. Similarly, mutants in *vegfaa* show a severe reduction in EC numbers and migration during ISV formation (Jin et al., 2017), phenotypes also seen in *VEGFA* mutant mice (Carmeliet *et al.*, 1996; Ferrara *et al.*, 1996). Therefore, it has been difficult in animal models to dissect out the individual contribution of a given gene or its downstream pathway components to either process.

Specific manipulations of ERK signaling in cultured ECs showed a requirement for DNA synthesis downstream of VEGFR2 activation, a process that was independent of PI3K activity (Takahashi *et al.*, 1999). However, deletion of ERK1 in mice did not result in vascular phenotypes (Pages et al., 1999), while knocking out ERK2 specifically in ECs in an ERK1^{-/-} background affected EC migration and proliferation (Srinivasan *et al.*, 2009). We showed that pERK is unchanged in *vegfab*^{nu155} mutants, despite defects in EC proliferation. It remains possible that our analysis missed a transitory change in ERK phosphorylation due to an endpoint staining. However, another study by Shin et al. (Shin *et al.*, 2016) suggests that in developing ISVs, ERK signaling rather controls EC migration with only small

effects on EC proliferation. A similar specific influence of ERK signaling on migration was reported in a HUVEC tube formation assay and for tumor ECs (Mavria et al., 2006). These results suggest that ERK phosphorylation can influence EC migration and/or proliferation depending on the developmental setting and the EC type analyzed.

Our work points towards a critical role of PI3K signaling for EC proliferation during ISV outgrowth. We find that blocking PI3K using different inhibitors selectively prevented ISV EC proliferation without influencing cell migration. This is in contrast to previous studies showing that PI3K signaling specifically affected EC migration in developing mouse embryos and in cultured ECs, with only minor effects on EC proliferation (Graupera *et al.*, 2008; Takahashi *et al.*, 1999). A previous study in zebrafish ISVs also showed that blocking PI3K signaling using the LY294002 inhibitor affected cell migration without reducing EC proliferation (Nicoli *et al.*, 2012). We directly imaged dividing cells using time-lapse imaging, while Nicoli et al. determined differences in BrdU incorporation. It might therefore be that PI3K signaling is important for cytokinesis with less effects on DNA synthesis, as previously shown in *Dictyostelium discoideum* cells (Janetopoulos et al., 2005). In addition, differences in the duration of PI3K inhibition will affect EC behaviors. We blocked PI3K signaling for 10 hours, while Graupera et al. analyzed vascular phenotypes after several days of removing PI3K 110alpha kinase function from ECs (Graupera *et al.*, 2008).

Other studies have shown that activating PI3K downstream of VEGF receptor signaling can lead to an increase in EC proliferation. Dayanir et al. generated a chimeric VEGF receptor 2 that could be activated using CSF-1 (Dayanir et al., 2001). When PI3K signaling was compromised, CSF-1 stimulation of this receptor failed to induce EC proliferation. Another study showed that Y1212 in VEGFR2 was important to control PI3K signaling pathway activation upstream of myc-dependent EC proliferation (Testini et al., 2019). In line with our observations in the mouse retina, blocking PI3K signaling in this setting reduced the number of phospho-histone 3 positive ECs (Ola *et al.*, 2016) and led to a reduction in EdU incorporation (Angulo-Urarte *et al.*, 2018). Importantly, activating mutations in PIK3CA can lead to venous malformations that are characterized by increased EC proliferation (Castel *et al.*, 2016; Castillo *et al.*, 2019; Castillo *et al.*, 2016). Together, these studies suggest a more important role of PI3K signaling in controlling EC proliferation downstream of Vegf signaling than previously anticipated.

However, our findings concerning the formation of the brain vasculature also point towards distinct functions of PI3 kinase signaling in different subsets of ECs, as we find no effect on BA sprouting or proliferation in embryos in which we inhibited PI3 kinase signaling. This was surprising, since BA formation relied on Vegfab signaling. BA formation was unaffected in *vegfaa^{mu128}* mutants, suggesting that Vegfab is the only ligand necessary for the formation of this blood vessel. This contrasts with ISV and CtA sprouting, where we find phenotypes in both *vegfaa^{mu128}* and *vegfab^{mu155}* mutants and a reduction in EC numbers when we inhibit PI3K signaling. Thus, distinct EC populations within developing zebrafish embryos rely on different signaling pathways in controlling their proliferative behaviors. Another open question is why blocking PI3K signaling in *vegfaa^{mu128}* mutants does not lead to a further reduction of CtA EC numbers, as double mutants for *vegfaa* and *vegfab* completely lack CtAs. This finding indicates that Vegfab activates other signaling

pathways in addition to PI3K during CtA formation. Further work will be necessary address these questions. Similarly, inhibition of PI3K signaling during ISV development did not reduce EC numbers to the baseline level observed in either uninjected or ctr. mRNA injected embryos (Fig. 7L). This might suggest that overexpressed *vegfab*₁₇₁ can activate another, PI3K independent, pathway and thereby induce EC proliferation. Alternatively, PI3K inhibition might not be complete in GDC-0326 treated embryos, as our western blots suggest (Supplementary Fig. 12) and still be activated to some extent through an increase in Vegfab signaling. It will be important in the future to distinguish between these possibilities.

One major drawback of our study is our current inability to visualize PI3K activation within newly sprouting ECs due to the lack of a robust immunohistochemistry protocol and how lack of *vegfab* gene function might affect these activation patterns. Thus, further work will be necessary to precisely determine in which EC populations and at which stages of the cell cycle PI3K signaling is required. An alternative hypothesis might be that Vegfab signaling regulates EC proliferation through another, PI3K signaling independent, pathway and that PI3K signaling might be activated through another upstream signaling pathway that is independent of VEGF. Of note, we still observed EC proliferation in PI3K inhibitor treated or *vegfab*^{mu155} mutant embryos, suggesting the existence of other signaling pathways contributing to ISV EC proliferation.

Why might Vegfab ligands affect EC proliferation without a major influence on EC migration? One reason for this could be due to the existence of differentially spliced VEGFA isoforms. In other species, all VEGFA isoforms are being generated by the same gene, while in zebrafish only *vegfaa* can generate both short and long, ECM binding, isoforms (Bahary *et al.*, 2007). *Vegfab* exclusively generates ECM binding isoforms. This setting allowed us to determine the unique effects of ECM binding VEGFA isoforms on EC behaviors during embryogenesis. Previous studies in developing mice (Ruhrberg *et al.*, 2002; Stalmans *et al.*, 2002), disease settings (Brash *et al.*, 2019; Cheng *et al.*, 1997; Guo *et al.*, 2001; Kazemi *et al.*, 2016) and in cultured ECs (Chen *et al.*, 2010; Delcombel *et al.*, 2013; Fearnley *et al.*, 2016; Herve *et al.*, 2005; Park *et al.*, 1993; Shiyong *et al.*, 2017) carefully investigated the effects of the different VEGFA isoforms on cellular behaviors (for review see (Peach *et al.*, 2018; Woolard *et al.*, 2009)). Some studies suggested that there are no differences in the ability of various VEGFA isoforms to support EC proliferation (Ruhrberg *et al.*, 2002), while others showed that ECs cultured on ECM derived from cells expressing VEGF189 or VEGF206 proliferated more strongly than those cultured in the presence of VEGF165 (Park *et al.*, 1993). Our studies support the latter findings by showing that matrix bound Vegfab isoforms can stimulate EC proliferation. We furthermore find that EC proliferation in *vegfab*^{mu155} mutants is more strongly affected in actively sprouting ECs in the forming CtAs and ISVs. We hypothesize that this might be due to the fact that during angiogenic growth ECs degrade the ECM, possibly releasing bound VEGF molecules, which would make them available to the invading ECs. Thus, the ability of long VEGF isoforms to associate with the ECM could provide a readily available growth factor pool within tissues.

MATERIALS AND METHODS

Zebrafish strains

Zebrafish were maintained as described previously (Westerfield, 1993). Transgenic lines and mutants used were *Tg(kdrl:EGFP)^{s843}*, *Tg(kdrl:Hsa.HRAS-mCherry)^{s916}*, *Tg(fli:nEGFP)^{y7}*, *vegfaa^{mu128}* (this study), *vegfab^{mu155}* (this study). References for zebrafish transgenic lines can be obtained on zfin.org. Adult zebrafish used in this study to generate embryos were between 1–2 years of age. Embryos were not selected for gender. All animal experiments were performed in compliance with the relevant laws and institutional guidelines and were approved by local animal ethics committees of the Landesamt für Natur, Umwelt und Verbraucherschutz Nordrhein-Westfalen. Animal protocols (number 806819) were further approved by the University of Pennsylvania Institutional Animal Care and Use Committee (IACUC).

Drug treatments

To inhibit PI3K, embryos were dechorionated and incubated in 10 uM LY-294002 hydrochloride (SIGMA) for 10 hours prior to imaging. To specifically inhibit PI3K 110 alpha, embryos were dechorionated and incubated in 10 uM, 25 uM or 50 uM of GDC-0326 (Cayman Chemical). To activate ERK signaling, embryos were dechorionated and incubated in 0.25 uM Phorbol-12-myristat-13-acetate (PMA) (SIGMA) for 4 hours prior to imaging.

Live imaging, confocal microscopy, and image processing

For *in vivo* imaging, live embryos were mounted in 1 % or 1.5 % low-melting-point agarose in E3 embryo medium with 168 mg l⁻¹ tricaine (1x) for anesthesia and 0.003 % phenylthiourea to inhibit pigmentation. Imaging was carried out on an inverted Leica SP5, Sp8 or a Zeiss LSM780 confocal microscope using a 20× dry objective. A heated microscope chamber at 28.5 °C was used for recording time-lapse videos. Stacks were taken every 15–20 min with a step size of 2 um. Confocal stacks and time-lapse videos were analyzed using IMARIS Software (Bitplane).

Generation of *vegfaa^{mu128}* and *vegfab^{mu155}* mutant zebrafish

Zinc-finger nucleases (ZFNs) against *vegfaa* were designed as previously described (Siekman et al., 2009). In the *vegfaa^{mu128}* allele, 7 nucleotides were deleted in exon 1 at the ZFN target site, resulting in an early stop codon after 18 amino acids. TALEN mutagenesis targeting *vegfab* was performed as described previously (Sugden et al., 2017). In the *vegfab^{mu155}* allele, 1 nucleotide was deleted and 2 nucleotides were inserted in exon 1 at the TALEN target site. This resulted in an early stop codon after 12 amino acids.

Genotyping

Primers for genotyping *vegfaa* were:

Vegfaa-fwd: 5' -GCTTCTTAATTGTTTTGAGAGCCAG- 3'

Vegfaa-rev: 5' -GGTGTGGGCTATTGCATTC- 3'

PCR products were digested with BccI (NEB). Fragment sizes are 116 bp + 123 bp for wild type allele and 239 bp for *vegfaa^{mu128}* allele.

Primers for genotyping *vegfab* were:

Vegfab-fwd: 5' -GGACCAACATGGGATTCTTG- 3'

Vegfab-rev: 5' -GGGTGGTCAGATATGCTCGT- 3'

PCR products were digested with BsrI (NEB). Fragment sizes are 188 bp + 221 bp for wild type allele and 409 bp for *vegfab^{mu155}* allele.

Cloning of *vegfab₁₇₁* and overexpression studies

Vegfab171 was amplified with primers

VEGFabattB1 ggggacaagttgtacaaaaagcagcgtGTTAAAAACGGGCAACGGCGG and VEGFab attB2 ggggaccactttgtacaagaagctgggtTCACCTCCTTGGTTTGTACACATCTGC from zebrafish 24 hpf cDNA. cDNA was generated using RNA that was isolated with RNeasy Plus Micro kit (Qiagen) from whole zebrafish embryos and reverse transcribed with iScript cDNA Synthesis Kit (BioRad). BP reaction was performed according to the manufacturer's instructions (ThermoFisher). Clones were verified by sequencing. *Vegfab₁₇₁* was then transferred into pCSDest (Villefranc et al., 2007) using LR cloning (ThermoFisher). Plasmid DNA was digested using NotI (NEB) and mRNA was generated using mMessage machine in vitro transcription kit (ThermoFisher). 50 pg of mRNA was injected into 1-cell stage zebrafish embryos. For control mRNA injections, we injected 50 pg of β -galactosidase mRNA (Vize et al., 1991).

In situ hybridization and fluorescence in situ hybridizations (FISH) with antibody staining

Whole-mount in situ hybridization was performed as previously described (Thisse and Thisse, 2008). Whole mount FISH combined with EGFP antibody staining was performed as previously described (Kochhan and Siekmann, 2013), using *Tg(kdrl:EGFP)^{s843}* fish. Probes for *vegfaa₁₂₁* (Lawson et al., 2002), *vegfab171* (Bahary et al., 2007), *dll4* (Siekmann and Lawson, 2007) and *flt4* (Lawson et al., 2001) were previously described.

Western blotting of zebrafish proteins

Dechorionated zebrafish embryos were de-yolked in Ginzburg buffer (55 mM NaCl, 1.8 mM KCl, 1.25 mM NaHCO₃) and lysed in Laemli buffer (20 embryos in 80 ul). Either 10 or 20 ul of sample were separated by 12 % SDS-PAGE and transferred onto PVDF membrane (Millipore). After blocking with 5 % Milk powder (Roth) in TBST, membranes were incubated with anti-phospho-p44/42 MAPK (Thr202/Tyr204) (1:1000; #8544; Cell Signaling), anti-p44/42 MAPK antibody (1:2000; #9102, Cell Signaling) and anti- α -Actin antibody (1:5000; A-5060, Sigma), Phospho-Akt (Ser473) (1:2000; #4060; Cell Signaling), Akt (1:1000; #9272; Cell Signaling). Primary antibodies were detected using mouse IgG HRP linked whole Ab (1:4000; NXA931; GE healthcare).

Immunostaining of zebrafish embryos

Immunostaining for phospho-p44/42 MAPK was performed as described previously (Costa *et al.*, 2016).

Mouse retina

To inhibit PI3K signaling, Pictilisib (GDC-0941, Selleckchem) stock solution was prepared by dissolving 8.5 mg of powder in 63 μ l DMSO. Before injection, 10 μ l of the stock solution was diluted in 190 μ l of corn oil to get a final concentration of 6,8 μ g/ μ l. 25 μ l of this solution (or vehicle only) was injected IP into each pup at P5 (55 mg/kg) and again 16 h later, before collecting the tissues at P6 (injections at -24 h and -8 h time points). To detect proliferating cells actively synthesizing DNA, EdU (Invitrogen - A10044) was injected IP 4 h before sacrifice; the signal was developed with the Click-it EdU Alexa Fluor 647 Imaging Kit.

Immunohistochemistry of mouse retinae

For mouse retina immunostaining, eyes were collected at the indicated time points and fixed in 4% PFA in PBS for 1h at room temperature (RT). After two PBS washes, retinae were micro-dissected and stained as described previously (Pontes-Quero *et al.*, 2019). Briefly, retinae were blocked and permeabilized with 0.3% Triton X-100, 3% FBS and 3% donkey serum in PBS. Samples were then washed twice in PBLEC buffer (1 mM CaCl_2 , 1 mM MgCl_2 , 1 mM MnCl_2 and 1% Triton X-100 in PBS). Biotinylated isolectinB4 (Vector Labs, B-1205, diluted 1:50) or primary antibodies (see below) were diluted in PBLEC buffer and tissues were incubated in this solution for 2 h at RT or overnight at 4°C. After five washes in blocking solution diluted 1:2, samples were incubated for 1 h at RT with Alexa-conjugated secondary antibodies (Molecular Probes). After two washes in PBS, retinae were mounted with Fluoromount-G (SouthernBiotech). To detect EdU-labelled DNA, an additional step was performed before mounting using the Click-It EdU kit (Thermo Fisher, C10340). Primary antibodies were used against the following proteins: Erg (AF-647, Abcam ab196149, 1:100), Phospho-S6 Ribosomal Protein (Ser235/236) (Cell Signaling Ab #4856, 1:100). The following secondary antibodies were used: Donkey anti-rabbit Cy3 (1:400, 711-167-003, Jackson ImmunoResearch) and Streptavidin Alexa 405 (1:400, S-32351, Thermofisher).

Western blot analysis of mouse proteins

For the analysis of protein expression, dissected organs were transferred to a reagent tube and frozen in liquid nitrogen. On the day of the immunoblotting the tissue was lysed with lysis buffer [(Tris-HCl pH=8 20 mM, EDTA 1 mM, DTT 1 mM, Triton X-100 1% and NaCl 150 mM, containing protease inhibitors (P-8340 Sigma) and phosphatase inhibitors (Calbiochem 524629) and orthovanadate-Na 1 mM)] and homogenized with a cylindrical glass pestle. Tissue/ cell debris was removed by centrifugation, and the supernatant was diluted in loading buffer and analyzed by SDS-PAGE and immunoblotting. Membranes were blocked with BSA and incubated with primary antibodies diluted 1/1000 against Cdh5/VE-cadherin (BD Biosciences 555289), Phospho-Akt (Cell Signaling, #4060S), Akt (Cell Signaling #9272S) or β -Actin (Santa Cruz Biotechnologies, sc-47778).

Microscopy of mouse retina

We used a Leica TCS SP8 confocal with a 405 nm laser and a white laser that allows excitation at any wavelength from 470nm to 670nm. All images shown are representative of the results obtained for each group and experiment. Littermates were dissected and processed under exactly the same conditions. Comparisons of phenotypes or signal intensity were made with pictures obtained using the same laser excitation and confocal scanner detection settings. Images were processed using ImageJ/Fiji and Adobe Photoshop.

Quantitative analysis of retinal vasculature

Single low magnification (10x lens) confocal fields of immunostained retinas were quantified with Fiji/ImageJ. Each microscopy field contained hundreds of ECs, and the relative or absolute number of cells in each field is indicated in the charts by a dot. As indicated in figure legends, microscopy images from several animals and retinas were used for the phenotypic comparisons and quantifications. Vascular IsolectinB4+ area and Erg+ or Edu+ cells were quantified semiautomatically using custom Fiji macros. EC density (EC number/mm²) was measured as the number of Erg+ cells relative to the vascularized IsolectinB4+ area in each field. The frequencies of Erg+ cells (ECs) in S-phase (EdU+) was determined as the ratio of double-positive cells to the total number of Erg+ cells per field.

Statistical analysis

Two groups of samples with a Gaussian distribution were compared by unpaired two-tailed Student's *t*-test. Comparisons among more than two groups were made by ANOVA followed by Tukey pairwise comparison. Column statistics were performed on data sets to check for normal distribution and appropriate tests to determine significance were performed using the Prism7 software. Each experiment was performed at least three times. Graphs represent mean \pm SD as indicated, and differences were considered significant at $p < 0.05$. All calculations were done in Excel and final datapoints analyzed and represented with GraphPad Prism. The sample size was chosen according to the observed statistical variation and published protocols. The experiments were not randomized, investigators were not blinded to allocation during experiments and outcome assessment and sample sizes were not predetermined.

Supplementary Material

Refer to Web version on PubMed Central for supplementary material.

ACKNOWLEDGEMENTS

We would like to thank Reinhild Bussmann, Mona Finch Stephen, Nadine Greer and Bill Vought for excellent fish care. In addition, we would like to thank Roman Tsaryk and Zeenat Diwan for critically reading of the manuscript and Caitlyn Parker for excellent technical assistance. We are grateful to Federica Lunella for help with the mouse retina dissection and immunohistochemistry. We would like to thank William Jones and Mary Mullins for providing the pCS2+ β -galactosidase plasmid. This work was funded by the Max-Planck-Society (A.F.S.), the Deutsche Forschungsgemeinschaft (DFG SI-1374/4-1, DFG SI-1374/5-1 and DFG SI-1374/6-1; A.F.S.) and start-up funds from the Cardiovascular Institute of the University of Pennsylvania Perelman School of Medicine (A.F.S.). We further acknowledge support from the Department of Cell and Developmental Biology of the University of Pennsylvania (A.F.S.). Work in R.B.'s lab was funded by the Ministerio de Economía, Industria y Competitividad (MEIC: SAF2017-89299-P and RYC-2013-13209) and the European Research Council (ERC-2014-StG - 638028 AngioGenesHD). This work was funded by NIH R01HL152086.

MATERIALS AVAILABILITY

All reagents and zebrafish lines generated in this study are available from the lead contact with a completed Materials Transfer Agreement.

REFERENCES

- Adams RH, and Alitalo K (2007). Molecular regulation of angiogenesis and lymphangiogenesis. *Nat Rev Mol Cell Biol* 8, 464–478. [PubMed: 17522591]
- Alvarez-Aznar A, Muhl L, and Gaengel K (2017). VEGF Receptor Tyrosine Kinases: Key Regulators of Vascular Function. *Curr Top Dev Biol* 123, 433–482. 10.1016/bs.ctdb.2016.10.001. [PubMed: 28236974]
- Angulo-Urarte A, Casado P, Castillo SD, Kobialka P, Kotini MP, Figueiredo AM, Castel P, Rajeev V, Mila-Guasch M, Millan J, et al. (2018). Endothelial cell rearrangements during vascular patterning require PI3-kinase-mediated inhibition of actomyosin contractility. *Nature communications* 9, 4826. 10.1038/s41467-018-07172-3.
- Bahary N, Goishi K, Stuckenholtz C, Weber G, Leblanc J, Schafer CA, Berman SS, Klagsbrun M, and Zon LI (2007). Duplicate VegfA genes and orthologues of the KDR receptor tyrosine kinase family mediate vascular development in the zebrafish. *Blood* 110, 3627–3636. blood-2006-04-016378 [pii] 10.1182/blood-2006-04-016378. [PubMed: 17698971]
- Bowler E, and Oltean S (2019). Alternative Splicing in Angiogenesis. *Int J Mol Sci* 20. 10.3390/ijms20092067.
- Brash JT, Denti L, Ruhrberg C, and Bucher F (2019). VEGF188 promotes corneal reinnervation after injury. *JCI Insight* 4. 10.1172/jci.insight.130979.
- Bussmann J, Wolfe SA, and Siekmann AF (2011). Arterial-venous network formation during brain vascularization involves hemodynamic regulation of chemokine signaling. *Development* 138, 1717–1726. 10.1242/dev.059881. [PubMed: 21429983]
- Carmeliet P, Ferreira V, Breier G, Pollefeyt S, Kieckens L, Gertsenstein M, Fahrig M, Vandenhoeck A, Harpal K, Eberhardt C, et al. (1996). Abnormal blood vessel development and lethality in embryos lacking a single VEGF allele. *Nature* 380, 435–439. 10.1038/380435a0. [PubMed: 8602241]
- Carmeliet P, Ng YS, Nuyens D, Theilmeier G, Brusselmans K, Cornelissen I, Ehler E, Kakkar VV, Stalmans I, Mattot V, et al. (1999). Impaired myocardial angiogenesis and ischemic cardiomyopathy in mice lacking the vascular endothelial growth factor isoforms VEGF164 and VEGF188. *Nat Med* 5, 495–502. [PubMed: 10229225]
- Casie Chetty S, Rost MS, Enriquez JR, Schumacher JA, Baltrunaite K, Rossi A, Stainier DY, and Sumanas S (2017). Vegf signaling promotes vascular endothelial differentiation by modulating *etv2* expression. *Dev Biol* 424, 147–161. 10.1016/j.ydbio.2017.03.005. [PubMed: 28279709]
- Castel P, Carmona FJ, Grego-Bessa J, Berger MF, Viale A, Anderson KV, Bague S, Scaltriti M, Antonescu CR, Baselga E, and Baselga J (2016). Somatic PIK3CA mutations as a driver of sporadic venous malformations. *Science translational medicine* 8, 332ra342. 10.1126/scitranslmed.aaf1164.
- Castillo SD, Baselga E, and Graupera M (2019). PIK3CA mutations in vascular malformations. *Curr Opin Hematol* 26, 170–178. 10.1097/MOH.0000000000000496. [PubMed: 30855339]
- Castillo SD, Tzouanacou E, Zaw-Thin M, Berenjano IM, Parker VE, Chivite I, Mila-Guasch M, Pearce W, Solomon I, Angulo-Urarte A, et al. (2016). Somatic activating mutations in *Pik3ca* cause sporadic venous malformations in mice and humans. *Science translational medicine* 8, 332ra343. 10.1126/scitranslmed.aad9982.
- Chen TT, Luque A, Lee S, Anderson SM, Segura T, and Iruela-Arispe ML (2010). Anchorage of VEGF to the extracellular matrix conveys differential signaling responses to endothelial cells. *J Cell Biol* 188, 595–609. 10.1083/jcb.200906044. [PubMed: 20176926]
- Cheng SY, Nagane M, Huang HS, and Cavenee WK (1997). Intracerebral tumor-associated hemorrhage caused by overexpression of the vascular endothelial growth factor isoforms VEGF121 and VEGF165 but not VEGF189. *Proc Natl Acad Sci U S A* 94, 12081–12087. 10.1073/pnas.94.22.12081. [PubMed: 9342366]

- Childs S, Chen JN, Garrity DM, and Fishman MC (2002). Patterning of angiogenesis in the zebrafish embryo. *Development* 129, 973–982. [PubMed: 11861480]
- Chung J, Grammer TC, Lemon KP, Kazlauskas A, and Blenis J (1994). PDGF- and insulin-dependent pp70S6k activation mediated by phosphatidylinositol-3-OH kinase. *Nature* 370, 71–75. 10.1038/370071a0. [PubMed: 8015612]
- Claesson-Welsh L (2016). VEGF receptor signal transduction - A brief update. *Vascul Pharmacol* 86, 14–17. 10.1016/j.vph.2016.05.011. [PubMed: 27268035]
- Costa G, Harrington KI, Lovegrove HE, Page DJ, Chakravartula S, Bentley K, and Herbert SP (2016). Asymmetric division coordinates collective cell migration in angiogenesis. *Nature cell biology* 18, 1292–1301. 10.1038/ncb3443. [PubMed: 27870831]
- Davies SP, Reddy H, Caivano M, and Cohen P (2000). Specificity and mechanism of action of some commonly used protein kinase inhibitors. *Biochem J* 351, 95–105. 10.1042/0264-6021:3510095. [PubMed: 10998351]
- Dayanir V, Meyer RD, Lashkari K, and Rahimi N (2001). Identification of tyrosine residues in vascular endothelial growth factor receptor-2/FLK-1 involved in activation of phosphatidylinositol 3-kinase and cell proliferation. *J Biol Chem* 276, 17686–17692. [PubMed: 11278468]
- Dejana E, Hirschi KK, and Simons M (2017). The molecular basis of endothelial cell plasticity. *Nature communications* 8, 14361. 10.1038/ncomms14361.
- Delcombel R, Janssen L, Vassy R, Gammons M, Haddad O, Richard B, Letourneur D, Bates D, Hendricks C, Waltenberger J, et al. (2013). New prospects in the roles of the C-terminal domains of VEGF-A and their cooperation for ligand binding, cellular signaling and vessels formation. *Angiogenesis* 16, 353–371. 10.1007/s10456-012-9320-y. [PubMed: 23254820]
- Fearnley GW, Smith GA, Abdul-Zani I, Yuldasheva N, Mughal NA, Homer-Vanniasinkam S, Kearney MT, Zachary IC, Tomlinson DC, Harrison MA, et al. (2016). VEGF-A isoforms program differential VEGFR2 signal transduction, trafficking and proteolysis. *Biology open* 5, 571–583. 10.1242/bio.017434. [PubMed: 27044325]
- Ferrara N, Carver-Moore K, Chen H, Dowd M, Lu L, O’Shea KS, Powell-Braxton L, Hillan KJ, and Moore MW (1996). Heterozygous embryonic lethality induced by targeted inactivation of the VEGF gene. *Nature* 380, 439–442. [PubMed: 8602242]
- Fish JE, Cantu Gutierrez M, Dang LT, Khyzha N, Chen Z, Veitch S, Cheng HS, Khor M, Antounians L, Njock MS, et al. (2017). Dynamic regulation of VEGF-inducible genes by an ERK/ERG/p300 transcriptional network. *Development* 144, 2428–2444. 10.1242/dev.146050. [PubMed: 28536097]
- Fujita M, Cha YR, Pham VN, Sakurai A, Roman BL, Gutkind JS, and Weinstein BM (2011). Assembly and patterning of the vascular network of the vertebrate hindbrain. *Development* 138, 1705–1715. 10.1242/dev.058776. [PubMed: 21429985]
- Gerber HP, McMurtrey A, Kowalski J, Yan M, Keyt BA, Dixit V, and Ferrara N (1998). Vascular endothelial growth factor regulates endothelial cell survival through the phosphatidylinositol 3'-kinase/Akt signal transduction pathway. Requirement for Flk-1/KDR activation. *J Biol Chem* 273, 30336–30343. 10.1074/jbc.273.46.30336. [PubMed: 9804796]
- Gimbrone MA Jr., and Garcia-Cardena G (2016). Endothelial Cell Dysfunction and the Pathobiology of Atherosclerosis. *Circ Res* 118, 620–636. 10.1161/CIRCRESAHA.115.306301. [PubMed: 26892962]
- Gong B, Liang D, Chew TG, and Ge R (2004). Characterization of the zebrafish vascular endothelial growth factor A gene: comparison with vegf-A genes in mammals and *Fugu*. *Biochimica et biophysica acta* 1676, 33–40. 10.1016/j.bbaexp.2003.10.006. [PubMed: 14732488]
- Graupera M, Guillermet-Guibert J, Foukas LC, Phng LK, Cain RJ, Salpekar A, Pearce W, Meek S, Millan J, Cutillas PR, et al. (2008). Angiogenesis selectively requires the p110alpha isoform of PI3K to control endothelial cell migration. *Nature* 453, 662–666. 10.1038/nature06892. [PubMed: 18449193]
- Graupera M, and Potente M (2013). Regulation of angiogenesis by PI3K signaling networks. *Exp Cell Res* 319, 1348–1355. 10.1016/j.yexcr.2013.02.021. [PubMed: 23500680]
- Guo P, Xu L, Pan S, Brekken RA, Yang ST, Whitaker GB, Nagane M, Thorpe PE, Rosenbaum JS, Su Huang HJ, et al. (2001). Vascular endothelial growth factor isoforms display distinct activities in

promoting tumor angiogenesis at different anatomic sites. *Cancer Res* 61, 8569–8577. [PubMed: 11731444]

- Heffron TP, Heald RA, Ndubaku C, Wei B, Augustin M, Do S, Edgar K, Eigenbrot C, Friedman L, Gancia E, et al. (2016). The Rational Design of Selective Benzoxazepin Inhibitors of the alpha-Isoform of Phosphoinositide 3-Kinase Culminating in the Identification of (S)-2-((2-(1-Isopropyl-1H-1,2,4-triazol-5-yl)-5,6-dihydrobenzo[f]imidazo[1,2-d][1,4]oxazepin-9-yl)oxy)propanamide (GDC-0326). *J Med Chem* 59, 985–1002. 10.1021/acs.jmedchem.5b01483. [PubMed: 26741947]
- Herve MA, Buteau-Lozano H, Mourah S, Calvo F, and Perrot-Applanat M (2005). VEGF189 stimulates endothelial cells proliferation and migration in vitro and up-regulates the expression of Flk-1/KDR mRNA. *Exp Cell Res* 309, 24–31. 10.1016/j.yexcr.2005.05.022. [PubMed: 15996656]
- Hogan BM, Bos FL, Bussmann J, Witte M, Chi NC, Duckers HJ, and Schulte-Merker S (2009). ccbe1 is required for embryonic lymphangiogenesis and venous sprouting. *Nature Genetics* 41, 396–398. Doi 10.1038/Ng.321. [PubMed: 19287381]
- Hogan BM, and Schulte-Merker S (2017). How to Plumb a Pisces: Understanding Vascular Development and Disease Using Zebrafish Embryos. *Dev Cell* 42, 567–583. 10.1016/j.devcel.2017.08.015. [PubMed: 28950100]
- Isogai S, Lawson ND, Torrealday S, Horiguchi M, and Weinstein BM (2003). Angiogenic network formation in the developing vertebrate trunk. *Development* 130, 5281–5290. [PubMed: 12954720]
- Janetopoulos C, Borleis J, Vazquez F, Iijima M, and Devreotes P (2005). Temporal and spatial regulation of phosphoinositide signaling mediates cytokinesis. *Dev Cell* 8, 467–477. 10.1016/j.devcel.2005.02.010. [PubMed: 15809030]
- Jin D, Zhu D, Fang Y, Chen Y, Yu G, Pan W, Liu D, Li F, and Zhong TP (2017). Vegfa signaling regulates diverse artery/vein formation in vertebrate vasculatures. *Journal of genetics and genomics = Yi chuan xue bao* 44, 483–492. 10.1016/j.jgg.2017.07.005. [PubMed: 29037991]
- Jin SW, Beisl D, Mitchell T, Chen JN, and Stainier DYR (2005). Cellular and molecular analyses of vascular tube and lumen formation in zebrafish. *Development* 132, 5199–5209. Doi 10.1242/Dev.02087. [PubMed: 16251212]
- Kazemi M, Carrer A, Moimas S, Zandona L, Bussani R, Casagrande B, Palmisano S, Prelazzi P, Giacca M, Zentilin L, et al. (2016). VEGF121 and VEGF165 differentially promote vessel maturation and tumor growth in mice and humans. *Cancer Gene Ther* 23, 125–132. 10.1038/cgt.2016.12. [PubMed: 27033458]
- Koch S, and Claesson-Welsh L (2012). Signal transduction by vascular endothelial growth factor receptors. *Cold Spring Harbor perspectives in medicine* 2, a006502. 10.1101/cshperspect.a006502. [PubMed: 22762016]
- Kochhan E, and Siekmann AF (2013). Zebrafish as a Model to Study Chemokine Function. In *Chemokines: Methods and Protocols*, Cardona EA, and Ubogu EE, eds. (Humana Press), pp. 145–159. 10.1007/978-1-62703-426-5_9.
- Lawson ND, Scheer N, Pham VN, Kim CH, Chitnis AB, Campos-Ortega JA, and Weinstein BM (2001). Notch signaling is required for arterial-venous differentiation during embryonic vascular development. *Development* 128, 3675–3683. [PubMed: 11585794]
- Lawson ND, Vogel AM, and Weinstein BM (2002). sonic hedgehog and vascular endothelial growth factor act upstream of the Notch pathway during arterial endothelial differentiation. *Dev Cell* 3, 127–136. [PubMed: 12110173]
- Liang D, Xu X, Chin AJ, Balasubramanian NV, Teo MA, Lam TJ, Weinberg ES, and Ge R (1998). Cloning and characterization of vascular endothelial growth factor (VEGF) from zebrafish, *Danio rerio*. *Biochimica et biophysica acta* 1397, 14–20. [PubMed: 9545518]
- Mavria G, Vercoulen Y, Yeo M, Paterson H, Karasarides M, Marais R, Bird D, and Marshall CJ (2006). ERK-MAPK signaling opposes Rho-kinase to promote endothelial cell survival and sprouting during angiogenesis. *Cancer Cell* 9, 33–44. 10.1016/j.ccr.2005.12.021. [PubMed: 16413470]
- Meadows KN, Bryant P, and Pumiglia K (2001). Vascular endothelial growth factor induction of the angiogenic phenotype requires Ras activation. *J Biol Chem* 276, 49289–49298. 10.1074/jbc.M108069200. [PubMed: 11682481]

- Mitchell P, Liew G, Gopinath B, and Wong TY (2018). Age-related macular degeneration. *Lancet* 392, 1147–1159. 10.1016/S0140-6736(18)31550-2. [PubMed: 30303083]
- Nagelberg D, Wang J, Su R, Torres-Vazquez J, Targoff KL, Poss KD, and Knaut H (2015). Origin, Specification, and Plasticity of the Great Vessels of the Heart. *Curr Biol* 25, 2099–2110. 10.1016/j.cub.2015.06.076. [PubMed: 26255850]
- Nakatsu MN, Sainson RC, Perez-del-Pulgar S, Aoto JN, Aitkenhead M, Taylor KL, Carpenter PM, and Hughes CC (2003). VEGF(121) and VEGF(165) regulate blood vessel diameter through vascular endothelial growth factor receptor 2 in an in vitro angiogenesis model. *Lab Invest* 83, 1873–1885. 10.1097/01.lab.0000107160.81875.33. [PubMed: 14691306]
- Nicoli S, Knyphausen CP, Zhu LJ, Lakshmanan A, and Lawson ND (2012). miR-221 is required for endothelial tip cell behaviors during vascular development. *Dev Cell* 22, 418–429. 10.1016/j.devcel.2012.01.008. [PubMed: 22340502]
- Ola R, Dubrac A, Han J, Zhang F, Fang JS, Larrivee B, Lee M, Urarte AA, Kraehling JR, Genet G, et al. (2016). PI3 kinase inhibition improves vascular malformations in mouse models of hereditary haemorrhagic telangiectasia. *Nature communications* 7, 13650. 10.1038/ncomms13650.
- Pages G, Guerin S, Grall D, Bonino F, Smith A, Anjuere F, Auberger P, and Pouyssegur J (1999). Defective thymocyte maturation in p44 MAP kinase (Erk 1) knockout mice. *Science* 286, 1374–1377. 10.1126/science.286.5443.1374. [PubMed: 10558995]
- Park JE, Keller GA, and Ferrara N (1993). The vascular endothelial growth factor (VEGF) isoforms: differential deposition into the subepithelial extracellular matrix and bioactivity of extracellular matrix-bound VEGF. *Mol Biol Cell* 4, 1317–1326. 10.1091/mbc.4.12.1317. [PubMed: 8167412]
- Peach CJ, Mignone VW, Arruda MA, Alcobia DC, Hill SJ, Kilpatrick LE, and Woolard J (2018). Molecular Pharmacology of VEGF-A Isoforms: Binding and Signalling at VEGFR2. *Int J Mol Sci* 19. 10.3390/ijms19041264.
- Potente M, Gerhardt H, and Carmeliet P (2011). Basic and therapeutic aspects of angiogenesis. *Cell* 146, 873–887. 10.1016/j.cell.2011.08.039. [PubMed: 21925313]
- Ricard N, Scott RP, Booth CJ, Velazquez H, Cilfone NA, Baylon JL, Gulcher JR, Quaggin SE, Chittenden TW, and Simons M (2019). Endothelial ERK1/2 signaling maintains integrity of the quiescent endothelium. *J Exp Med* 216, 1874–1890. 10.1084/jem.20182151. [PubMed: 31196980]
- Roman BL, Pham VN, Lawson ND, Kulik M, Childs S, Lekven AC, Garrity DM, Moon RT, Fishman MC, Lechleider RJ, and Weinstein BM (2002). Disruption of *acvr1l* increases endothelial cell number in zebrafish cranial vessels. *Development* 129, 3009–3019. [PubMed: 12050147]
- Rossi A, Gauvrit S, Marass M, Pan L, Moens CB, and Stainier DYR (2016). Regulation of Vegf signaling by natural and synthetic ligands. *Blood* 128, 2359–2366. 10.1182/blood-2016-04-711192. [PubMed: 27557946]
- Ruhrberg C, Gerhardt H, Golding M, Watson R, Ioannidou S, Fujisawa H, Betsholtz C, and Shima DT (2002). Spatially restricted patterning cues provided by heparin-binding VEGF-A control blood vessel branching morphogenesis. *Genes Dev* 16, 2684–2698. 10.1101/gad.242002. [PubMed: 12381667]
- Schuermann A, Helker CS, and Herzog W (2014). Angiogenesis in zebrafish. *Semin Cell Dev Biol* 31, 106–114. 10.1016/j.semcdb.2014.04.037. [PubMed: 24813365]
- Shin M, Beane TJ, Quillien A, Male I, Zhu LJ, and Lawson ND (2016). Vegfa signals through ERK to promote angiogenesis, but not artery differentiation. *Development* 143, 3796–3805. 10.1242/dev.137919. [PubMed: 27578780]
- Shiying W, Boyun S, Jianye Y, Wanjun Z, Ping T, Jiang L, and Hongyi H (2017). The Different Effects of VEGFA121 and VEGFA165 on Regulating Angiogenesis Depend on Phosphorylation Sites of VEGFR2. *Inflamm Bowel Dis* 23, 603–616. 10.1097/MIB.0000000000001055. [PubMed: 28296822]
- Siekmann AF, and Lawson ND (2007). Notch signalling limits angiogenic cell behaviour in developing zebrafish arteries. *Nature* 445, 781–784. Doi 10.1038/Nature05577. [PubMed: 17259972]
- Siekmann AF, Standley C, Fogarty KE, Wolfe SA, and Lawson ND (2009). Chemokine signaling guides regional patterning of the first embryonic artery. *Gene Dev* 23, 2272–2277. Doi 10.1101/Gad.1813509. [PubMed: 19797767]

- Simons M, and Eichmann A (2015). Molecular controls of arterial morphogenesis. *Circ Res* 116, 1712–1724. 10.1161/CIRCRESAHA.116.302953. [PubMed: 25953926]
- Simons M, Gordon E, and Claesson-Welsh L (2016). Mechanisms and regulation of endothelial VEGF receptor signalling. *Nat Rev Mol Cell Biol* 17, 611–625. 10.1038/nrm.2016.87. [PubMed: 27461391]
- Srinivasan R, Zabuawala T, Huang H, Zhang J, Gulati P, Fernandez S, Karlo JC, Landreth GE, Leone G, and Ostrowski MC (2009). Erk1 and Erk2 regulate endothelial cell proliferation and migration during mouse embryonic angiogenesis. *PLoS One* 4, e8283. 10.1371/journal.pone.0008283. [PubMed: 20011539]
- Stalmans I, Ng YS, Rohan R, Fruttiger M, Bouche A, Yuce A, Fujisawa H, Hermans B, Shani M, Jansen S, et al. (2002). Arteriolar and venular patterning in retinas of mice selectively expressing VEGF isoforms. *J Clin Invest* 109, 327–336. [PubMed: 11827992]
- Sugden WW, Meissner R, Aegerter-Wilmsen T, Tsaryk R, Leonard EV, Bussmann J, Hamm MJ, Herzog W, Jin Y, Jakobsson L, et al. (2017). Endoglin controls blood vessel diameter through endothelial cell shape changes in response to haemodynamic cues. *Nature cell biology* 19, 653–665. 10.1038/ncb3528. [PubMed: 28530658]
- Takahashi T, Ueno H, and Shibuya M (1999). VEGF activates protein kinase C-dependent, but Ras-independent Raf-MEK-MAP kinase pathway for DNA synthesis in primary endothelial cells. *Oncogene* 18, 2221–2230. [PubMed: 10327068]
- Taylor JS, Braasch I, Frickey T, Meyer A, and Van de Peer Y (2003). Genome duplication, a trait shared by 22000 species of ray-finned fish. *Genome research* 13, 382–390. 10.1101/gr.640303. [PubMed: 12618368]
- Taylor JS, Van de Peer Y, Braasch I, and Meyer A (2001). Comparative genomics provides evidence for an ancient genome duplication event in fish. *Philos Trans R Soc Lond B Biol Sci* 356, 1661–1679. 10.1098/rstb.2001.0975. [PubMed: 11604130]
- Testini C, Smith RO, Jin Y, Martinsson P, Sun Y, Hedlund M, Sainz-Jaspeado M, Shibuya M, Hellstrom M, and Claesson-Welsh L (2019). Myc-dependent endothelial proliferation is controlled by phosphotyrosine 1212 in VEGF receptor-2. *EMBO Rep* 20, e47845. 10.15252/embr.201947845. [PubMed: 31545012]
- Thisse C, and Thisse B (2008). High-resolution in situ hybridization to whole-mount zebrafish embryos. *Nat Protoc* 3, 59–69. 10.1038/nprot.2007.514. [PubMed: 18193022]
- Ulrich F, Ma LH, Baker RG, and Torres-Vazquez J (2011). Neurovascular development in the embryonic zebrafish hindbrain. *Dev Biol* 357, 134–151. 10.1016/j.ydbio.2011.06.037. [PubMed: 21745463]
- Vempati P, Popel AS, and Mac Gabhann F (2014). Extracellular regulation of VEGF: isoforms, proteolysis, and vascular patterning. *Cytokine Growth Factor Rev* 25, 1–19. 10.1016/j.cytogfr.2013.11.002. [PubMed: 24332926]
- Viallard C, and Larrivee B (2017). Tumor angiogenesis and vascular normalization: alternative therapeutic targets. *Angiogenesis* 20, 409–426. 10.1007/s10456-017-9562-9. [PubMed: 28660302]
- Villefranc JA, Amigo J, and Lawson ND (2007). Gateway compatible vectors for analysis of gene function in the zebrafish. *Dev Dyn* 236, 3077–3087. 10.1002/dvdy.21354. [PubMed: 17948311]
- Vize PD, Melton DA, Hemmati-Brivanlou A, and Harland RM (1991). Assays for gene function in developing *Xenopus* embryos. *Methods Cell Biol* 36, 367–387. 10.1016/s0091-679x(08)60288-5. [PubMed: 1811145]
- Vlahos CJ, Matter WF, Hui KY, and Brown RF (1994). A specific inhibitor of phosphatidylinositol 3-kinase, 2-(4-morpholinyl)-8-phenyl-4H-1-benzopyran-4-one (LY294002). *J Biol Chem* 269, 5241–5248. [PubMed: 8106507]
- Westerfield M (1993). *The zebrafish book : a guide for the laboratory use of zebrafish (Brachydanio rerio)* (M. Westerfield).
- Wong TY, Cheung CM, Larsen M, Sharma S, and Simo R (2016). Diabetic retinopathy. *Nat Rev Dis Primers* 2, 16012. 10.1038/nrdp.2016.12. [PubMed: 27159554]
- Woolard J, Bevan HS, Harper SJ, and Bates DO (2009). Molecular diversity of VEGF-A as a regulator of its biological activity. *Microcirculation* 16, 572–592. 10.1080/10739680902997333. [PubMed: 19521900]

Workman P, Clarke PA, Raynaud FI, and van Montfort RL (2010). Drugging the PI3 kinome: from chemical tools to drugs in the clinic. *Cancer Res* 70, 2146–2157. 10.1158/0008-5472.CAN-09-4355. [PubMed: 20179189]

Author Manuscript

Author Manuscript

Author Manuscript

Author Manuscript

- *Vegfab* zebrafish mutants show defects in endothelial cell proliferation in distinct blood vessels
- Inhibition of PI3 kinase signaling leads to similar defects in endothelial cell proliferation
- Overexpression of *vegfab* leads to an increase in endothelial cell proliferation
- Blood vessel plasticity can rescue vascular phenotypes in *vegfab* mutants

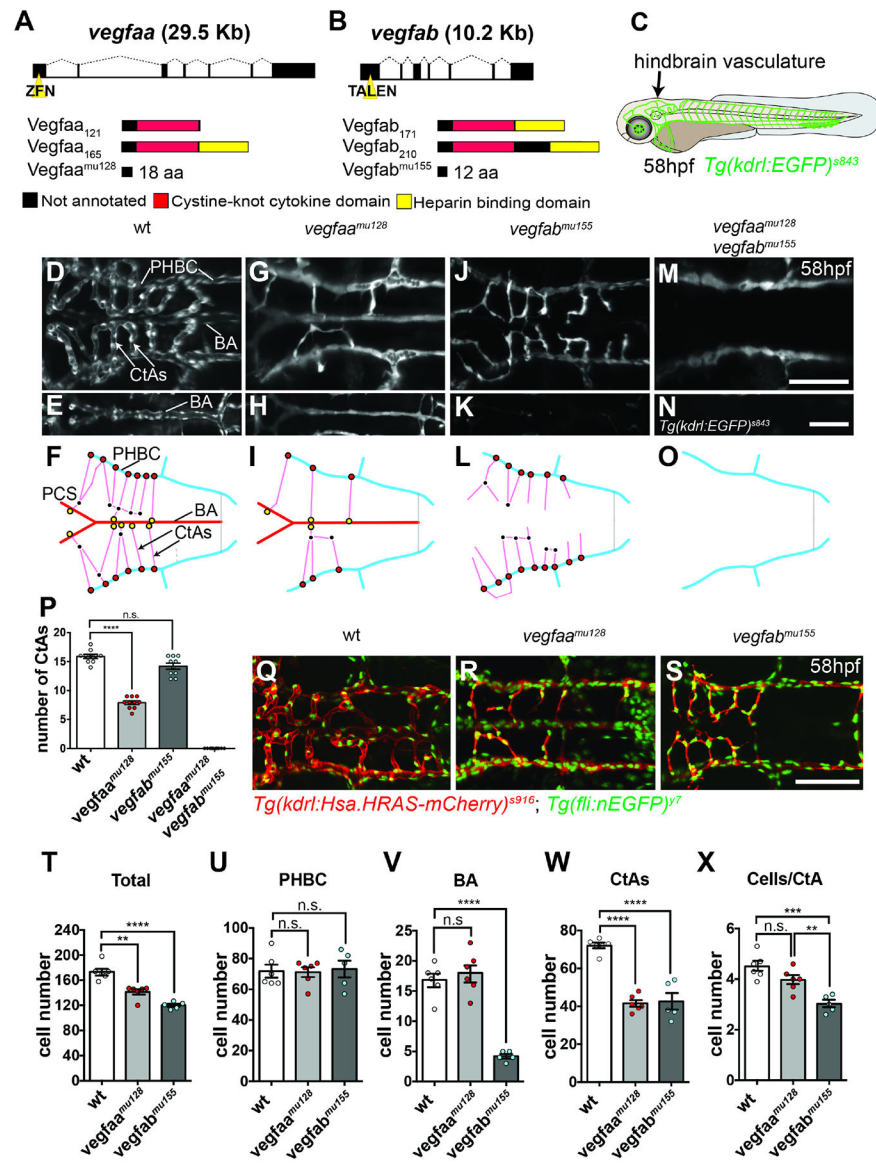


Figure 1. Mutations in *vegfaa* and *vegfab* affect hindbrain blood vessel formation.

(A-B) Schematic representation of zinc finger nuclease or TALEN target site at the genomic sequence for *vegfaa* (A) and *vegfab* (B). Black boxes in the gene structure represent exons and dashed lines represent introns, yellow triangle indicates the position of the targeting sites. Protein domains are displayed below in comparison with wt protein. Black boxes represent sequences that are not annotated, red boxes are cysteine-knot cytokine domains and yellow boxes are heparin binding domains. (C) Cartoon of 58 hpf embryo, arrow indicates imaged region. (D-N) Maximum intensity projection of confocal z-stacks of *Tg(kdrl:EGFP)^{s843}* wild type (D), *vegfaa^{mu128}* (G), *vegfab^{mu155}* (J) and double mutant (M) embryos at 58 hpf. Smaller rectangular panels (E, H, K and N) show cropped ventral region of the maximum intensity projection for better visualization of the basilar artery (BA). Dorsal views, anterior to the left. Scale bar = 100 μ m. (F, I, L, O) Graphical representation of hindbrain vascular phenotypes, indicating the position of

Primordial hindbrain channel (PHBC)-Central artery (CtA) connections (red filled circles), CtA-CtA connections (black dots) and CtA-BA-Posterior Communicating segments (PCS) connections (yellow filled circles). (P) Quantification of CtA number in wt (n = 10), *vegfaa^{mu128}* (n=10), *vegfab^{mu155}* (n=10) and double mutant embryos (n = 10). Values are mean±s.d.; n.s = not significant; **** p<0.0001. Groups were compared by ANOVA followed by Tukey pairwise comparison.

(Q-S) Maximum intensity projections of confocal z-stacks of *Tg(kdrl:Hsa.HRAS-mCherry)^{s916}*; *(fli:nEGFP)^{y7}* wt (Q), *vegfaa^{mu128}* (R) and *vegfab^{mu155}* embryos (S) at 58 hpf. Dorsal view, anterior to the left. Scale bar = 100 um. (T-X) Quantification of the total cell numbers (T) as well as cells in the PHBC (U), BA (V) CtAs (W) and cells per CtA (X), for wt embryos (n=6) compared to *vegfaa^{mu128}* (n=6) and *vegfab^{mu155}* (n=5) mutants. Dots represent individual embryos; black lines indicate the mean value±s.d.; n.s = not significant; ** p<0.01; *** p<0.001; **** p<0.0001. Groups were compared by ANOVA followed by Tukey pairwise comparison.

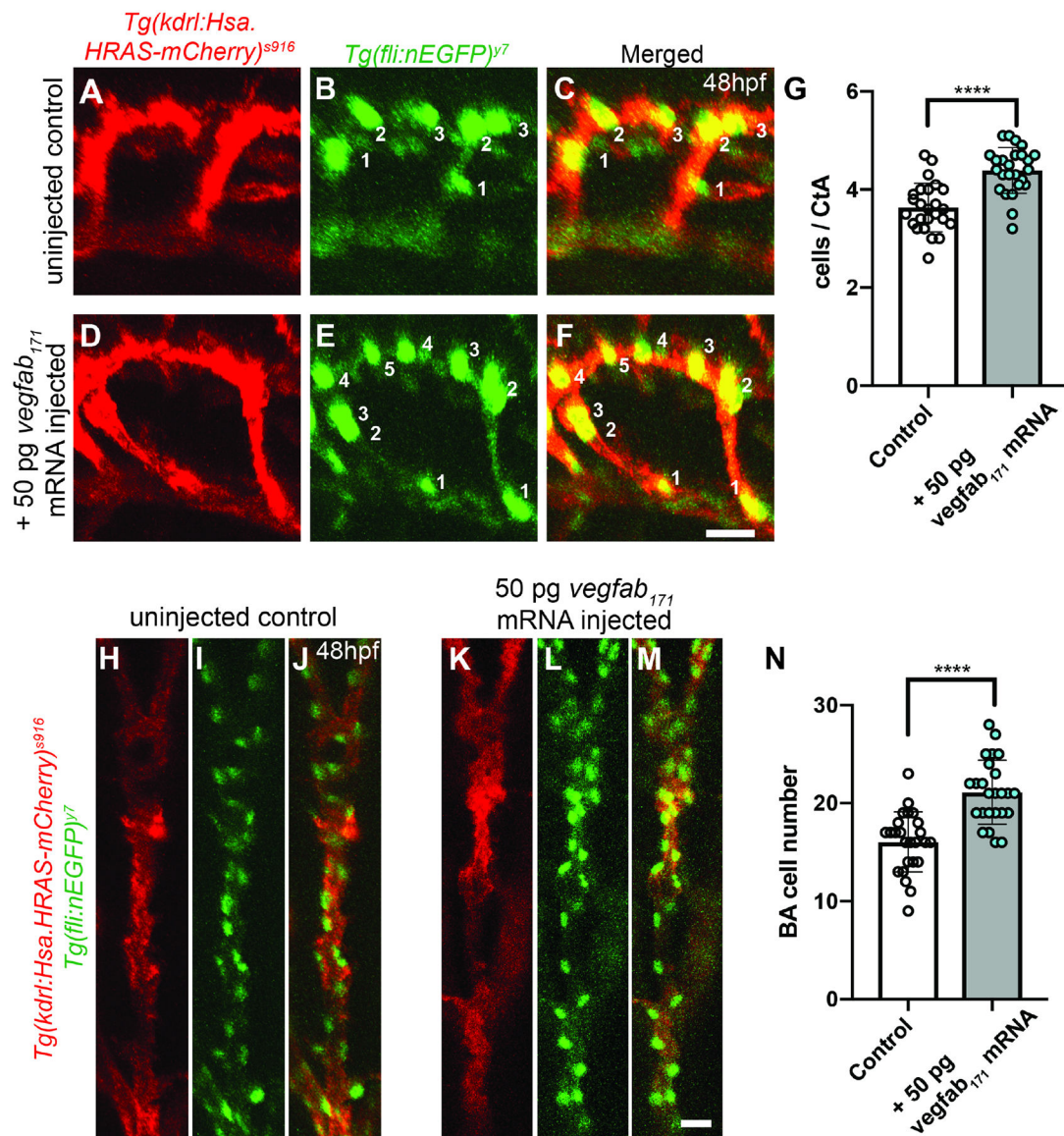


Figure 2. *Vegfab₁₇₁* overexpression increases EC proliferation in the BA and CtAs. (A-F) Maximum intensity projection of a confocal z-stack showing CtAs in 48 hpf $Tg(kdrl:Hsa.HRAS-mCherry)^{s916}$; $Tg(fli:nEGFP)^{y7}$ control embryos (A-C) or 50 pg $vegfab_{171}$ mRNA injected embryos (D-F). Dorso-lateral views; anterior to the left. Scale bar = 25 μ m. (G) Quantification of cells per CtA in control (n=25) and 50 pg $vegfab_{171}$ mRNA injected embryos (n=25). Dots represent individual embryos; black lines indicate the mean value \pm s.d.; **** p < 0.0001. Groups were compared by unpaired two-tailed Student's *t*-test. (H-M) Maximum intensity projection of a confocal z-stack of BA in 48 hpf $Tg(kdrl:Hsa.HRAS-mCherry)^{s916}$; $Tg(fli:nEGFP)^{y7}$ control embryos (H-J) and 50 pg $vegfab_{171}$ mRNA injected embryos (K-M). Dorsal view; anterior to the top. Scale bar = 25 μ m. (N) Quantification of BA cell numbers in control (n=25) and 50 pg $vegfab_{171}$ mRNA injected embryos (n=25). Dots represent individual embryos; black lines indicate the mean value \pm s.d. **** p < 0.0001. Groups were compared by unpaired two-tailed Student's *t*-test.

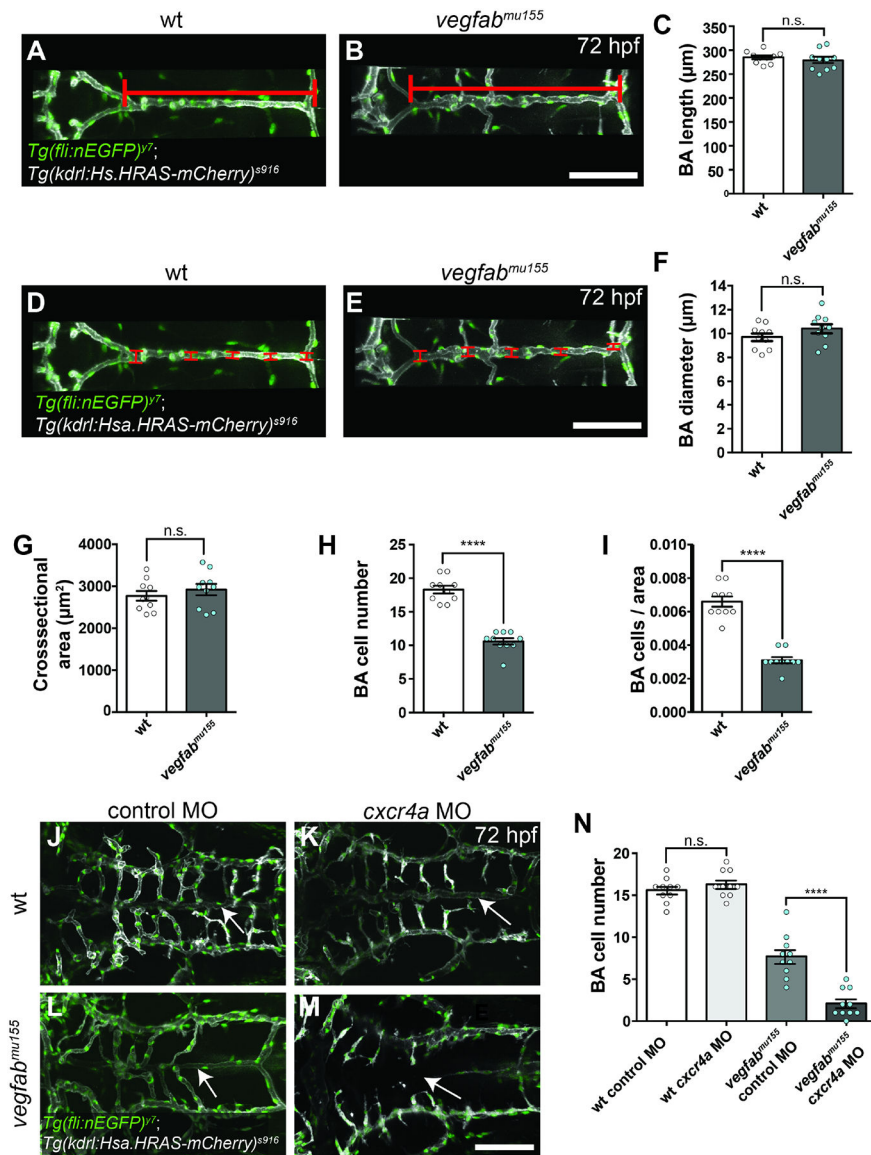


Figure 3. Rescue of BA formation in *vegfab*^{mu155} mutants through EC recruitment from CtAs in a *cxcr4a* dependent manner.

(A, B, D, E) Maximum intensity projection of a confocal z-stack of BA in *Tg(kdrl:Hsa.HRAS-mCherry)*^{s916}; *Tg(fli:nEGFP)*^{y7} wt embryos (A and D) or *vegfab*^{mu155} mutant embryos (B and E) at 72 hpf. Red line indicates the measured area. Dorsal views; anterior to the left. Scale bar = 100 μm. (C, F) Quantification of BA length (C) and diameter (F) in wt (n=10) and *vegfab*^{mu155} (n=10). Dots represent individual embryos; black lines indicate the mean value ±s.d. n.s = not significant. Groups were compared by unpaired two-tailed Student's *t*-test. (G-I) Quantification of BA cross-sectional area (G), BA cell numbers (H) and BA cells per area (I) in wt (n=10) and *vegfab*^{mu155} (n=10). Dots represent individual embryos; black lines indicate the mean value ±s.d. n.s = not significant. Groups were compared by unpaired two-tailed Student's *t*-test. (J-M) Maximum intensity projection of a confocal z-stack of the hindbrain vasculature of *Tg(kdrl:Hsa.HRAS-mCherry)*^{s916}; *Tg(fli:nEGFP)*^{y7} wild type embryos (J-K) or *vegfab*^{mu155}

(L-M) control morpholino (J and L) or *cxcr4a* morpholino injected embryos (K and M) at 72 hpf. Arrows point to BA location. Dorsal view; anterior to the left. Scale bar = 100 μ m. (N) Quantification of BA cell number at 72 hpf in control morpholino (n=10), *cxcr4a* morpholino (n=10), *vegfab^{mu155}* control morpholino (n=10) or *vegfab^{mu155} cxcr4a* morpholino injected embryos. Dots represent individual embryos; black lines indicate the mean value \pm s.d. n.s = not significant; **** p<0.0001. Groups were compared by ANOVA followed by Tukey pairwise comparison.

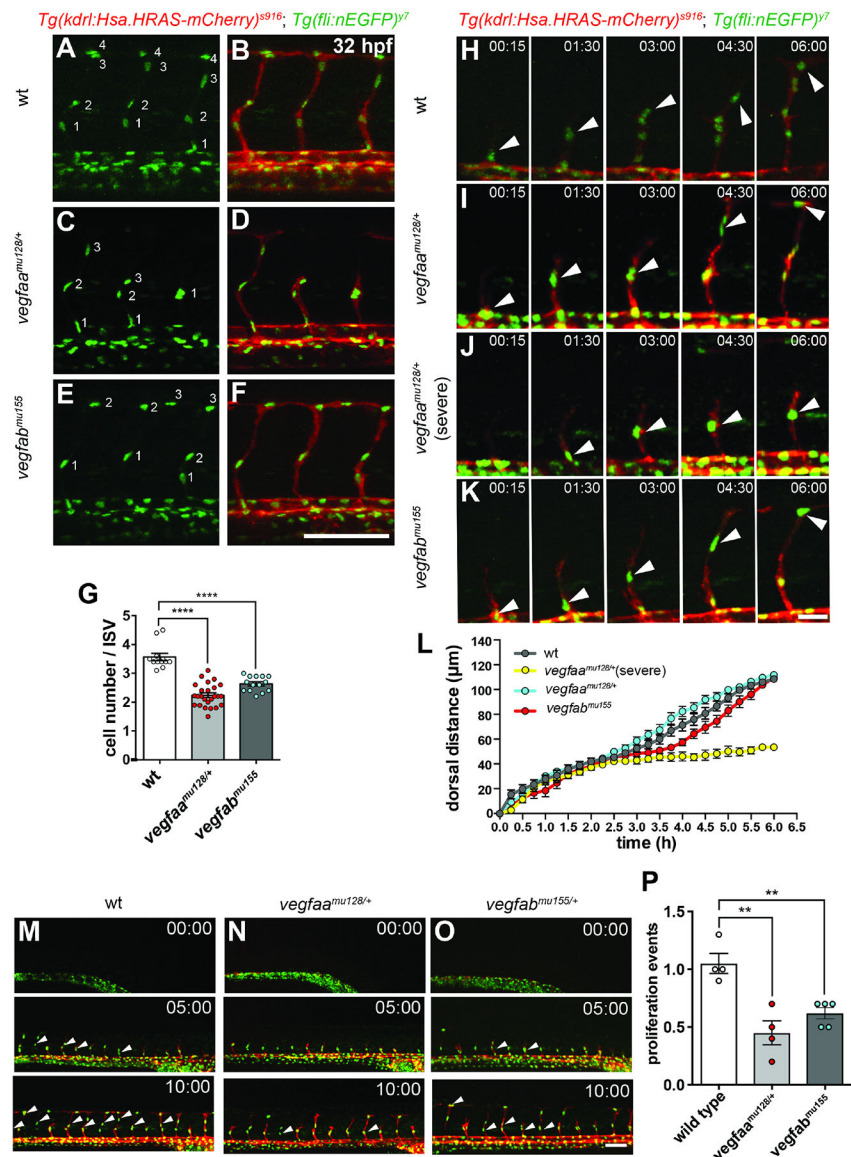


Figure 4. Analysis of EC migration and proliferation in the trunk vasculature of *vegfaa^{mu128}* and *vegfab^{mu155}* mutants.

(A-F) Maximum intensity projections of confocal z-stacks of *Tg(kdrl:Hsa.HRAS-mCherry)^{s916}; (fli:nEGFP)^{y7}* wt (A-B), *vegfaa^{mu128/+}* (C-D) and *vegfab^{mu155}* (E-F) embryos; lateral view, anterior to the left. Scale bar = 100 μ m. (G) Quantification of EC numbers per intersegmental blood vessel sprout (ISV) in wt (n=12), *vegfaa^{mu128/+}* (n=26) and *vegfab^{mu155}* (n=14) mutants at 32 hpf. Dots represent individual embryos; black lines indicate the mean value \pm s.d.; **** p<0.0001. Groups were compared by ANOVA followed by Tukey pairwise comparison. (H-K) Confocal time-lapse images of individual sprouting ISV showing tip cell migration (arrowheads) in wt (H), *vegfaa^{mu128/+}* (I), severely affected *vegfaa^{mu128/+}* (J) and *vegfab^{mu155}* (K) embryos; lateral views, anterior to the left. Scale bar = 20 μ m. (L) Quantification of tip cell migration, measuring the dorsal movement of cell nuclei for wt (grey; n=13 ISVs, 4 embryos), *vegfaa^{mu128/+}* (blue; n=11 ISVs, 4 embryos), *vegfaa^{mu128/+}* severe (yellow; n=11 ISVs, 4 embryos) and *vegfab^{mu155}* (red; n=11 ISVs,

4 embryos). Values are mean \pm s.d. (M-O) Confocal time-lapse images of 10 growing ISVs in wt (M), *vegfaa*^{mu128/+} (N) and *vegfab*^{mu155} (O) embryos (n=4 each) that were analyzed for cell proliferation. Arrowheads indicate cells derived from proliferation. Lateral views, anterior to the left. Scale bar = 100 μ m. (P) Quantification of proliferation events per ISV during 10 h of time lapse imaging from 22hpf in wt (n=40 ISVs, 4 embryos), *vegfaa*^{mu128/+} (n=40 ISVs, 4 embryos) and *vegfab*^{mu155} (n=50 ISVs, 5 embryos). Dots represent individual embryos; black lines indicate the mean value \pm s.d.; ** p<0.01. Groups were compared by ANOVA followed by Tukey pairwise comparison.

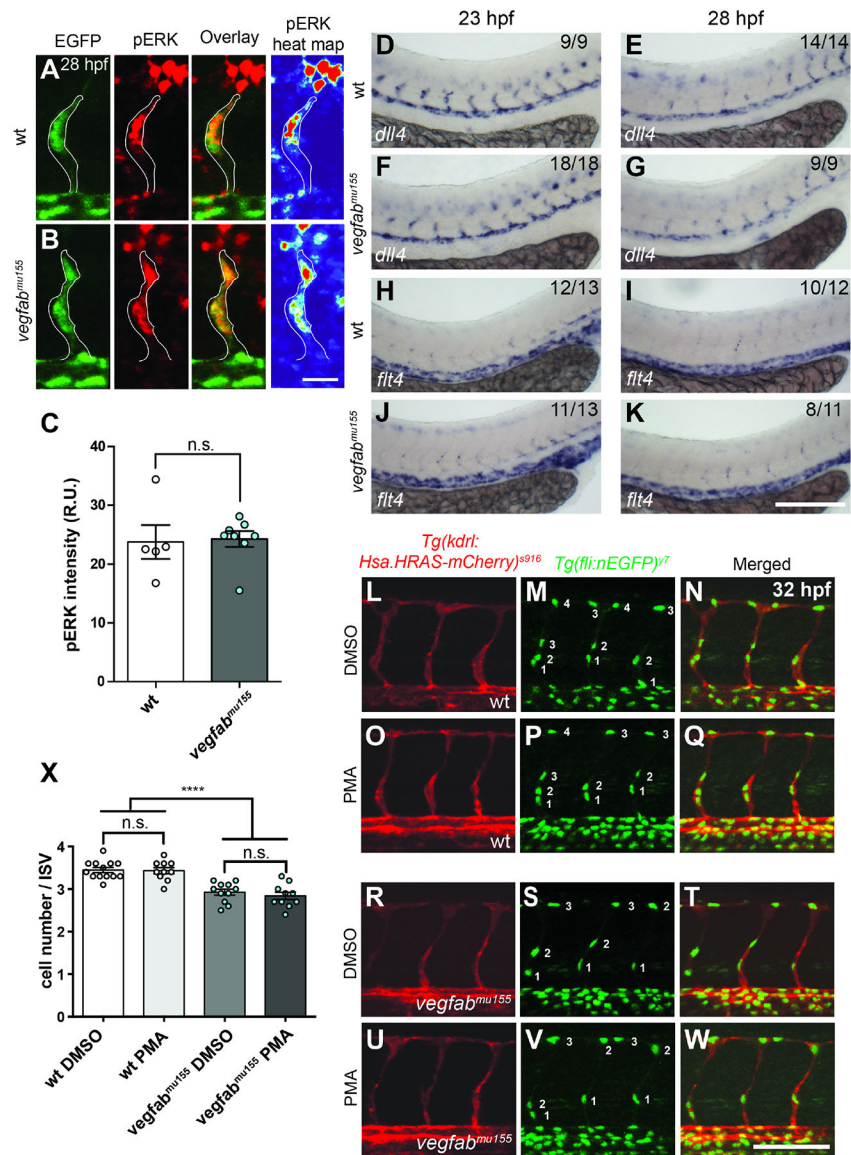


Figure 5. *Vegfab* is not essential for ERK phosphorylation or *dll4* and *flt4* expression in sprouting ISVs.

(A-B) High magnification of confocal z-stack of anti-pERK antibody staining in transgenic *Tg(fli:nEGFP)^{y7}* embryos with quantitative heat map of pERK staining at 28 hpf for wt (A) and *vegfab^{mu155}* (B) embryos, lateral views, anterior to the left. Scale bar = 20 μ m. (C) Quantification of pERK staining intensity of every ISV cell represented in relative units (R.U.) for wt (n=5) and *vegfab^{mu155}* (n=8) at 28 hpf. Dots represent individual embryos; black lines indicate the mean value \pm s.d. n.s. = not significant. Groups were compared by unpaired two-tailed Student's *t*-test. (D-K) Whole mount in situ hybridization for *dll4* (D-G) and *flt4* (H-K) on wt (D-E and H-I) and *vegfab^{mu155}* (F-G and J-K) embryos at 23 or 28 hpf. Lateral views, anterior to the left. Scale bar = 100 μ m. (L-Q) Maximum intensity projections of *Tg(kdrl:Hsa.HRAS-mCherry)^{s916}, (fli:nEGFP)^{y7}* wt embryos treated with DMSO (L-N) or with 0.25 μ m PMA (O-Q). (R-W) Maximum intensity projections of *Tg(kdrl:Hsa.HRAS-mCherry)^{s916}, (fli:nEGFP)^{y7}* *vegfab^{mu155}* embryos treated with DMSO

(R-T) or *vegfab^{mu155}* embryos treated with PMA (U-W). Lateral views, anterior to the left. Scale bar = 100 μ m. (X) Quantification of EC numbers of wt embryos treated with DMSO (n=13) or PMA (n=10) and *vegfab^{mu155}* embryos treated with DMSO (n=11) or PMA (n=10). Dots represent individual embryos; black lines indicate the mean value \pm s.d.; **** p<0.0001. Scale bar=100 μ m. Groups were compared by ANOVA followed by Tukey pairwise comparison.

Author Manuscript

Author Manuscript

Author Manuscript

Author Manuscript

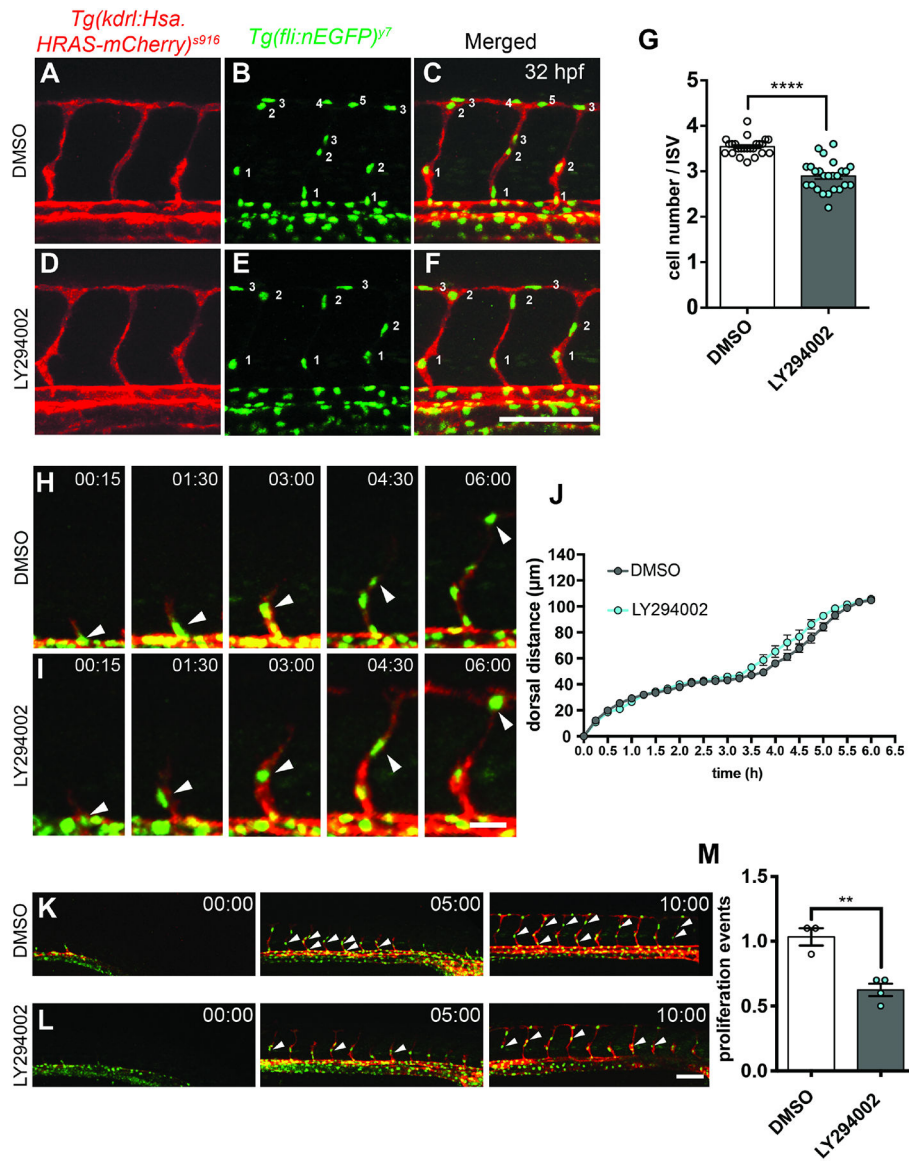


Figure 6. LY294002 mediated PI3K inhibition affects EC proliferation.

(A-F) Maximum intensity projection of a confocal z-stack of the trunk vasculature of *Tg(kdrl:Hsa.HRAS-mCherry)^{s916}; (fli:nEGFP)^{y7}* wt embryos treated with DMSO (A-C) or 10 μ M LY294002 (D-F) at 32 hpf. Lateral views, anterior to the left. Scale bar = 100 μ m. (G) Quantification of cells per ISV in DMSO treated embryos (n=24) compared to LY294002 treated embryos (n=25). Dots represent individual embryos; black lines indicate the mean value \pm s.d. **** p<0.0001. Groups were compared by unpaired two-tailed Student's *t*-test. (H, I) Confocal time-lapse images of individual sprouting ISV showing tip cell migration (arrowheads) in wt embryos treated with DMSO (H) or LY294002 (I) starting from 22 hpf for 6 h. Lateral views, anterior to the left. Scale bar = 20 μ m. (J) Quantification of tip cell migration, measuring the dorsal movement of cell nuclei for wt embryos treated with DMSO (grey; 11 ISVs, 3 embryos) or LY294002 (blue; 11 ISVs, 4 embryos); Values are mean \pm s.d. (K, L) Confocal time-lapse images of 10 growing ISVs

in embryos treated with DMSO (K) or with LY294002 (L) that were analyzed for cell proliferation. Arrowheads indicate cells derived from proliferation. Lateral views, anterior to the left. Scale bar = 100 μ m. (M) Quantification of proliferation events in ISVs during 10 h of time lapse imaging from 22 – 32 hpf after DMSO (n=30 ISVs, 3 embryos) or LY294002 (n=40 ISVs, 4 embryos) treatment. Dots represent individual embryos; black lines indicate the mean value \pm s.d.; ** p<0.01. Groups were compared by unpaired two-tailed Student's *t*-test.

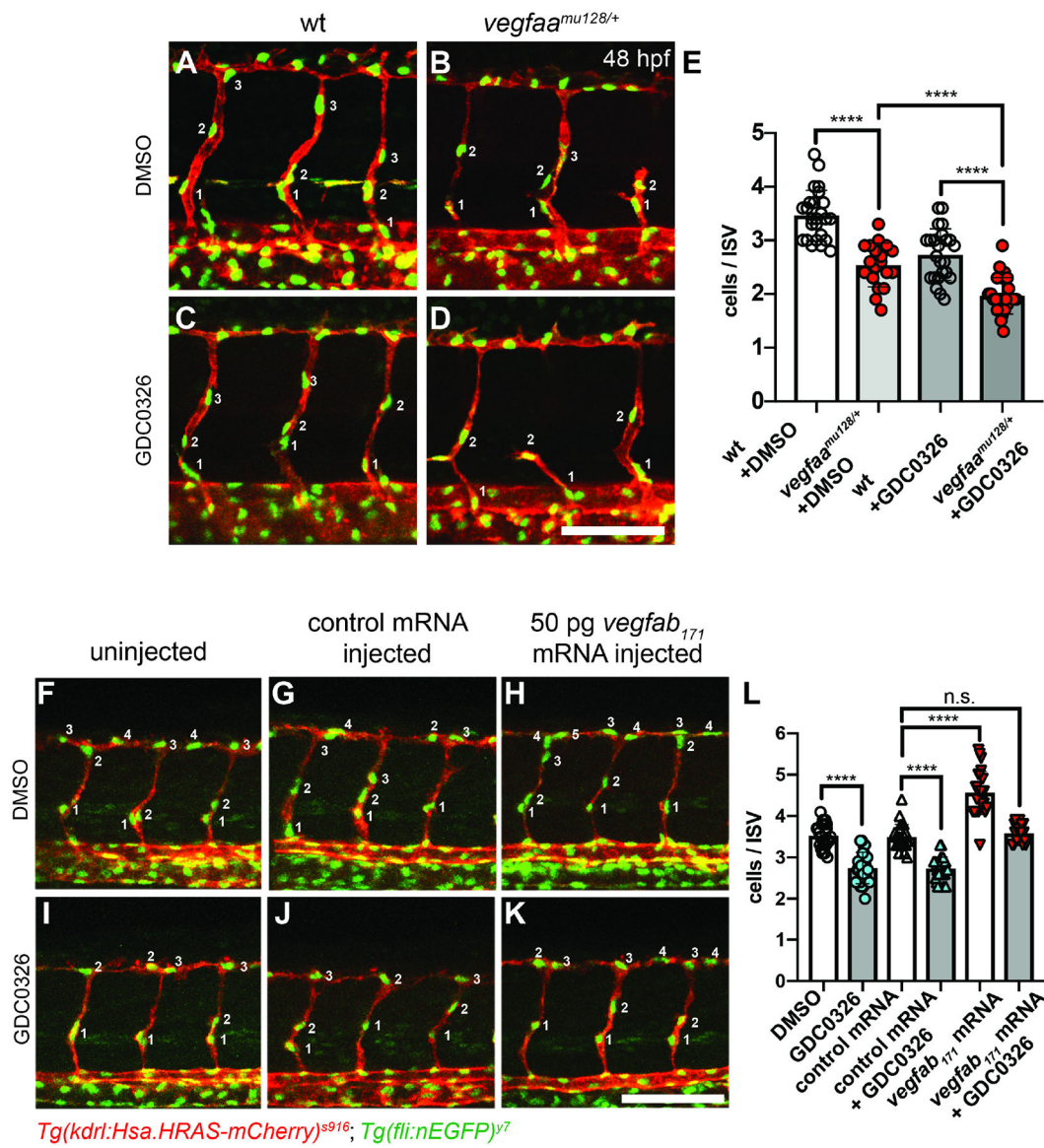


Figure 7. VEGFAB can act through PI3K signaling to influence EC proliferation.

(A-D) Maximum intensity projections of confocal z-stacks of the trunk vasculature of double transgenic *Tg(kdrl:Hsa.HRAS-mCherry)^{s916}; Tg(fli1a:nEGFP)^{y7}* wt embryos (A and C) or *vegfaa^{mu128/+}* embryos (B and D) at 48 hpf, treated with either DMSO (A-B) or GDC0326 (C-D). Lateral view; anterior to the left. Scale bar = 100 μ m. (E) Quantification of cells per ISV in wt embryos treated with DMSO (n=25), *vegfaa^{mu128/+}* embryos treated with DMSO (n=19), wt embryos treated with GDC0326 (n=24) and *vegfaa^{mu128/+}* embryos treated with GDC0326 (n=25). Dots represent individual embryos; black lines indicate the mean value \pm s.d. **** p<0.0001. Groups were compared by ANOVA followed by Tukey pairwise comparison. (F-K) Maximum intensity projection of a confocal z-stack of the trunk vasculature of double transgenic *Tg(kdrl:Hsa.HRAS-mCherry)^{s916}; Tg(fli1a:nEGFP)^{y7}* DMSO treated embryos (F-H) or GDC0326 treated embryos (I-K) at 32 hpf, either uninjected control (F and I), ctr. mRNA injected (G and J) or *vegfab₁₇₁* mRNA injected

(H and K). Lateral view; anterior to the left. Scale bar = 100 μ m. (L) Quantification of cells per ISV in uninjected DMSO treated embryos (n=25), ctr. mRNA injected and DMSO treated (n=25), *vegfab*₁₇₁ mRNA injected and DMSO treated (n=25), uninjected GDC0326 treated (n=25), ctr. mRNA injected GDC0326 treated (n=25) and *vegfab*₁₇₁ mRNA injected treated with GDC0326 (n=25). Dots represent individual embryos; black lines indicate the mean value \pm s.d. n.s = not significant; **** p <0.0001. Groups were compared by ANOVA followed by Tukey pairwise comparison.

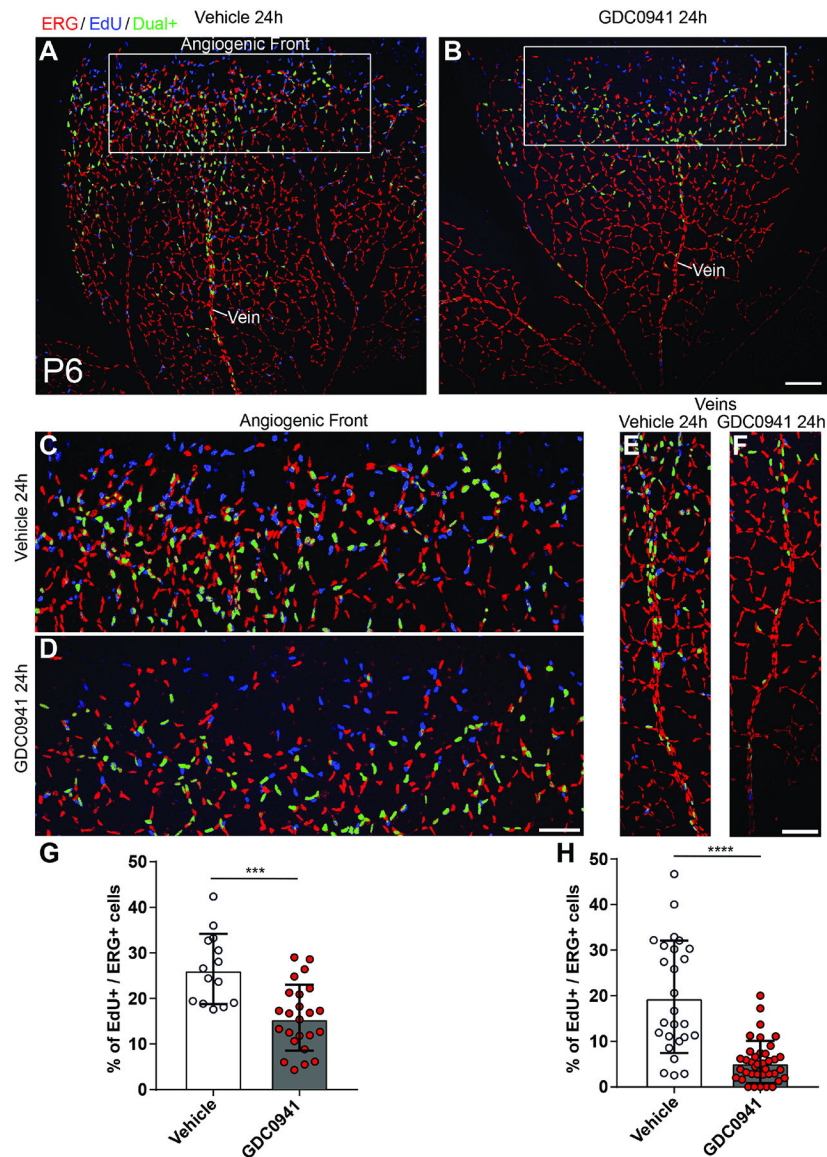


Figure 8. Inhibiting PI3 kinase signaling during retinal angiogenesis reduces EC proliferation. (A) Representative confocal micrograph of a vehicle treated P6 retina. EC nuclei are labelled in red by ERG, EdU incorporation in blue and overlay of red and blue channels is pseudocolored in green. Boxed area is magnified in (C). (B) Representative confocal micrograph of a GDC-0941 treated P6 retina. Boxed area is magnified in (D). Scale bar = 150 μ m. (C) Magnified image of angiogenic front in vehicle treated retina. (D) Magnified image of GDC-0941 treated retina. (E) Magnified image of vehicle treated vein. (F) Magnified image of GDC-0941 treated vein. (G) Quantification of percentage of EdU positive ERG positive cells in vehicle or GDC-0941 treated retinas at the angiogenic front. Each dot represents a retina flank. For vehicle treated group (n=4; 7 retinas), for GDC-0941 treated group (n=5; 10 retinas). Groups were compared by unpaired two-tailed Student's *t*-test; black lines indicate the mean value \pm s.d.; *** $p < 0.001$.

(H) Quantification of percentage of EdU positive ERG positive cells in vehicle or GDC-0941 treated retinas in the vein area. Each dot represents a retina flank. For vehicle treated group (n=4; 7 retinas), for GDC-0941 treated group (n=5; 10 retinas). Groups were compared by unpaired two-tailed Student's *t*-test; black lines indicate the mean value \pm s.d; **** $p < 0.0001$.